

Award Number: W81XWH-16-1-0256

TITLE: Regressing Atherosclerosis by Resolving Plaque
Inflammation

PRINCIPAL INVESTIGATOR: Dr. Png Loke Ph.D.

CONTRACTING ORGANIZATION: New York University School of Medicine
New York, NY 10016

REPORT DATE: July 2018

TYPE OF REPORT: Annual

PREPARED FOR: U.S. Army Medical Research and Materiel Command
Fort Detrick, Maryland 21702-5012

DISTRIBUTION STATEMENT:

Approved for public release; distribution
unlimited

The views, opinions and/or findings contained in this report are those of the author(s) and should not be construed as an official Department of the Army position, policy or decision unless so designated by other documentation.

REPORT DOCUMENTATION PAGE				Form Approved OMB No. 0704-0188	
Public reporting burden for this collection of information is estimated to average 1 hour per response, including the time for reviewing instructions, searching existing data sources, gathering and maintaining the data needed, and completing and reviewing this collection of information. Send comments regarding this burden estimate or any other aspect of this collection of information, including suggestions for reducing this burden to Department of Defense, Washington Headquarters Services, Directorate for Information Operations and Reports (0704-0188), 1215 Jefferson Davis Highway, Suite 1204, Arlington, VA 22202-4302. Respondents should be aware that notwithstanding any other provision of law, no person shall be subject to any penalty for failing to comply with a collection of information if it does not display a currently valid OMB control number. PLEASE DO NOT RETURN YOUR FORM TO THE ABOVE ADDRESS.					
1. REPORT DATE July 2018		2. REPORT TYPE Annual		3. DATES COVERED 1 Jul 2017 - 30 Jun 2018	
4. TITLE AND SUBTITLE Regressing Atherosclerosis by Resolving Plaque Inflammation				5a. CONTRACT NUMBER	
				5b. GRANT NUMBER W81XWH-16-1-0256	
				5c. PROGRAM ELEMENT NUMBER	
6. AUTHOR(S) Dr. Png Loke E-Mail: Png.Loke@nyumc.org				5d. PROJECT NUMBER	
				5e. TASK NUMBER	
				5f. WORK UNIT NUMBER	
7. PERFORMING ORGANIZATION NAME(S) AND ADDRESS(ES) New York University School of Medicine 430 East 29 th Street New York, NY 10016				8. PERFORMING ORGANIZATION REPORT NUMBER	
9. SPONSORING / MONITORING AGENCY NAME(S) AND ADDRESS(ES) U.S. Army Medical Research and Materiel Command Fort Detrick, Maryland 21702-5012				10. SPONSOR/MONITOR'S ACRONYM(S)	
				11. SPONSOR/MONITOR'S REPORT NUMBER(S)	
12. DISTRIBUTION / AVAILABILITY STATEMENT Approved for Public Release; Distribution Unlimited					
13. SUPPLEMENTARY NOTES					
14. ABSTRACT Macrophages play key roles in progression of atherosclerosis. Our goal is to understand the mechanisms by which atherosclerosis can be clinically regressed by altering the macrophage state in the plaques to resolve the inflammation, as well as to develop new therapeutic strategies to promote atherosclerosis regression by altering the macrophage activation state. We have found that successful atherosclerosis regression requires the alteration of macrophages in the plaques to a tissue repair "alternatively" activated state. This switch in activation state requires the action of TH2 cytokines interleukin (IL)-4 or IL-13. To accomplish our goals, we are testing if these molecules, or derivative of these molecules, will be able to accelerate atherosclerosis regression in mouse models. Additionally, we will develop nanomedicines that can favorably and rapidly affect the content and inflammatory state of macrophages in atherosclerotic plaques to promote regression. Concurrently, we will characterize the macrophages to understand the mechanisms that promote atherosclerosis regression.					
15. SUBJECT TERMS None provided					
16. SECURITY CLASSIFICATION OF:			17. LIMITATION OF ABSTRACT UU	18. NUMBER OF PAGES 27	19a. NAME OF RESPONSIBLE PERSON USAMRMC
a. REPORT U	b. ABSTRACT U	c. THIS PAGE U			19b. TELEPHONE NUMBER (include area code)

Table of Contents

	<u>Page</u>
1. Introduction.....	1
2. Keywords.....	1
3. Accomplishments.....	1
4. Impact.....	
5.Changes/Problems.....	9
6. Products.....	9
7.Participants & Other Collaborating Organizations.....	9
8.Special Reporting Requirements.....	10
9. Appendices.....	attached

1. INTRODUCTION

We currently have a limited capacity to **reverse** the high level of atherosclerotic plaques already present in the population. Our vision is to harness the immune system to reverse atherosclerosis. Inadequate resolution of inflammation is fundamental to all stages of atherosclerosis, with macrophages playing key roles in progression of the disease. The goal of our proposal is to understand the mechanisms by which atherosclerosis can be clinically regressed by altering the macrophage state in the plaques to resolve the inflammation, as well as to develop new therapeutic strategies to promote atherosclerosis regression by altering the macrophage activation state. By understanding and harnessing these mechanisms in mouse models of atherosclerosis, the final goal would be to develop new immunotherapeutic approaches that can complement existing lipid lowering treatments, thereby providing benefits to veterans, who experience a high rate of cardiovascular disease. We have recently found that successful atherosclerosis regression requires the alteration of macrophages in the plaques from an inflammatory “classically” activated state to a tissue repair “alternatively” activated state. This switch in activation state requires the action of T_H2 cytokines interleukin (IL)-4 or IL-13. To accomplish our goals, we are testing if these molecules, or derivative of these molecules, will be able to accelerate atherosclerosis regression in mouse models. Additionally, we will develop nanomedicines that can favorably and rapidly affect the content and inflammatory state of macrophages in atherosclerotic plaques to promote regression. Concurrently, we will characterize the macrophages to understand the mechanisms that promote atherosclerosis regression.

2. KEYWORDS: Atherosclerosis, cardiovascular disease, macrophages, interleukin 4, interleukin 13, nanoparticles.

3. ACCOMPLISHMENTS:

The major goals and objectives of the project are:

Specific Aim 1: To determine the mechanism(s) regulating inflammation resolution in regressing plaques and to promote resolution by administration of T_H2 cytokines (IL-4 and IL-13).

To accomplish this aim, the Major Tasks are:

- (1) Determine the requirement for IL-4 in mediating M2 activation and regression and to generate conditional STAT6 deficient animals to independently determine the requirement for the IL-4 signaling pathway in specific cell types, including macrophages.
- (2) Determine the cellular source of IL-4 in mediating M2 activation and regression.
- (3) Determine the optimal dosage of IL-4 or IL-13 required in vivo for M2 activation of peritoneal macrophages without adverse effects.

- (4) Determine the optimal dosage and efficacy of IL-4 or IL-13 required in vivo to promote plaque regression.
- (5) Generate ATAC-seq data from M2 macrophages from atherosclerosis plaques.
- (6) Generate RNA-seq data from M2 macrophages from atherosclerosis plaques.
- (7) Integrate ATAC-seq and RNA-seq data to build a transcriptional network for M2 activation in regressing plaques.

Specific Aim 2: To develop nanomedicines to favorably and rapidly affect the content and inflammatory state of macrophages in atherosclerotic plaques.

To accomplish this aim, the Major Tasks are:

- (1) Determine the efficacy of nanoparticles containing LXR agonist to promote plaque regression.
- (2) Characterize changes to plaque macrophages after treatment with LXR-agonist-NP.
- (3) Determine the efficacy of nanoparticles containing Netrin1- and Unc5b-siRNA to promote plaque regression.
- (4) Characterize changes to plaque macrophages after treatment with Netrin1- and Unc5b-siRNA -NP.

What was accomplished under these goals?

Major activities for this reporting period:

Aim 1 Major Tasks

Major Task 1 Determine the requirement and source of IL-4 required for atherosclerosis regression.

Major Task 1a: Fisher lab: Determine the requirement for IL-4 for atherosclerosis regression.

- We used 2 independent mouse models to investigate the role of IL4 and IL13 in atherosclerosis regression. In the first model, atherosclerosis is developed and regressed in mice lacking both IL4 and IL13 (IL4/13 DKO), to examine whether these cytokines play any role in regression. In the second model, only cells that are newly recruited to plaques during the regression phase are deficient in IL4/13.

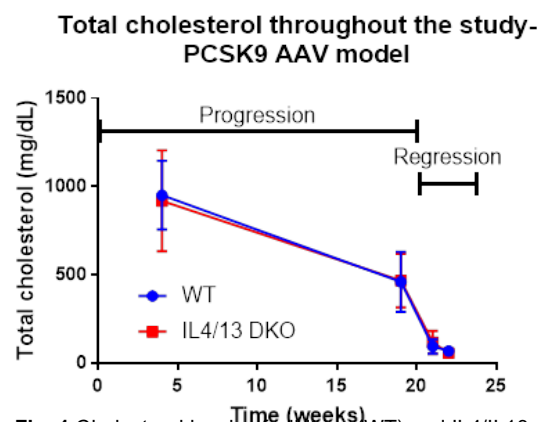


Fig. 1 Cholesterol levels of wildtype (WT) and IL4/IL13 double knockout (DKO) mice are AAV-PCSK9 injection and feeding on a Western Diet. The results show that absence of IL4/IL13 does not have an effect on cholesterol levels compared to WT mice.

- For the first atherosclerosis model, we treated 24 wildtype (WT) and 27 IL4/13 double knockout (DKO) mice with an AAV expressing a hyper-active form of the PCSK9 gene and fed the mice on a Western Diet (WD). After 4 weeks post AAV injection and Western diet feeding, serum cholesterol levels were raised to above 900mg/dL. After 19 weeks post AAV injection, serum cholesterol levels were ~470mg/dL, which were still hypercholesterolemic enough to promote atherosclerosis progression. WT and IL4/IL13 DKO mice had similar cholesterol levels throughout the study (Figure 1). Half of the mice were sacrificed after 20 weeks of Western diet feeding to determine baseline levels of plaques between WT and IL4/IL13 DKO mice. The other half of the mice were induced to undergo atherosclerosis regression by treating them with an antisense oligonucleotide (ASO) to ApoB and switching them to a normal chow diet. Cholesterol levels in both the WT and IL4/IL13 DKO mice were markedly decreased to below 100mg/dL following this treatment and remained low throughout the regression phase. After 3 weeks of regression, aortic roots and arches were harvested (Figure 2)

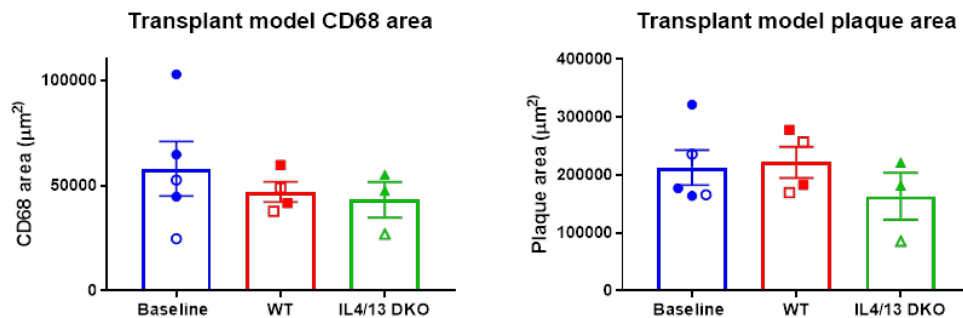


Fig. 2. The absence of IL4/IL13 does not significantly alter plaque regression. AAV-PCSK9 treated WT and IL4/IL13DKO mice were fed a western diet to develop plaques, and then half of the mice were induced to undergo atherosclerosis regression by treatment with ApoB ASO and switching onto a normal chow diet, compared to the baseline group. The results show no significant effects of IL4/IL13 deficiency on plaque regression compared to WT mice.

- We are currently processing the tissues for morphometric analysis and RNA investigation using laser-capture microdissection. Something does not jive here- we say they analyses are in progress, yet Figure 2 legend says there is no effect on regression. Also the figure shown, which may not be Figure 2, indicates a transplant study, which is not a ASO study.
- For the second atherosclerosis regression model, we conducted an aortic transplant study, whereby 12 LDLr KO mice were fed a Western diet for 20 weeks, after which their aortic arches were harvested. Five arches were embedded to generate frozen sections and serve as the baseline group and another 7 arches were transplanted into WT or IL4/13 DKO recipients. After 2 weeks arches were harvested and processed for morphometric analysis. Our results show that the control regression group (WT recipients) had ~20% less macrophage content than baseline plaques. Since our previous studies demonstrated a significantly greater decrease in

CD68 area between baseline plaques and the control regression group, we decided to extend the period of regression to 4 weeks. These studies are ongoing and we already harvested 5 WT and 5 IL4/13 DKO transplant recipients, with 15 more in the various groups to be harvested soon. The harvested aortic arches are currently being processed for morphometric analysis and RNA investigations.

Major Task 1b: Fisher and Loke labs: Generate conditional STAT6 deficient animals to independently determine the requirement for the IL-4 signaling pathway in specific cell types, including macrophages.

- We received conditional STAT6 deficient animals from Ingenious Targeting Laboratories. After rederivation into our animal facility we are currently in the process of crossing these animals to macrophage specific Cre expressing mice. We are crossing them to CD169-Cre to delete STAT6 in tissue resident macrophages and CX3CR1-Cre and CSF1R-Cre mice to delete them in all other macrophages. The crosses are in progress at the moment.

Major Task 2: Fisher Lab: Determine the cellular source of IL-4 in mediating M2 activation and regression.

- We used the IL-4 reporter 4GET mice (as a marker of the cellular source of IL-4) to examine IL-4 producing cells in both the surgical aortic transplant model, as well as the non-surgical AAV-PCSK9 model system. We found that the predominant IL-4 producing cells are eosinophils in the aortic transplant model, whereas with the AAV-PCSK9 system, CD4+ T cells were the predominant source of IL-4. However, we did not observe any significant differences in the number of IL-4 producing cells under atherosclerosis progression and regression conditions with the non-surgical AAV-PCSK9 system. Hence, we may get a more direct answer as to whether recruited cells are required to produce IL-4 from the experiments described in Major Task 1, than through the utilization of the IL-4 reporter system. We are focusing on the cause-effect relationship experiments through the transplantation of aorta into IL-4/IL-13 deficient mice as an alternative strategy.

Major Task 3: Loke lab: Determine the optimal dosage of IL-4 or IL-13 required *in vivo* for M2 activation of peritoneal macrophages without adverse effects.

- In the previous funding period, we had optimized the dosage of IL-4 and IL-13 for the treatment of plaques and are now addressing Major Task 4.

Major Task 4: Loke lab: Determine the optimal dosage and efficacy of IL-4 or IL-13 required *in vivo* to promote plaque regression.

- We discovered and published that monocyte derived macrophages are the main source of M2 macrophages required for atherosclerosis regression {Rahman, 2017 #1337} and developed a better mouse model for characterization of these macrophages during atherosclerosis. We use a “fate-mapping” approach to track monocyte derived macrophages {Gundra, 2017 #1299}, which can be combined with a (PCSK9)-encoding adeno-associated viral vector system {Peled, 2017 #1338}, for better precision without genetic crosses onto the LDLR^{-/-} background. Utilizing this system, we can isolate tdTomato positive macrophages for downstream analysis.
- We have performed two independent experiments utilizing these tdTomato – PCSK9 mice to develop and then regress atherosclerosis. In the first experiment, we utilized a **2 week** atherosclerosis regression strategy. In the second experiment, we utilized a **4 week** atherosclerosis regression strategy. The protocol was adapted for the second experiment because the IL-4 treatment for the 2 week experiment did not perform as expected (see below).
- For the first experiment (2 week treatment), we treated 17 *Cx3cr1*-Cre Rosa flox-tdTomato mice (9 females and 8 males) with an AAV expressing a hyper-active form of the PCSK9 gene and fed the mice on a Western Diet (WD). Serum cholesterol levels were monitored at 2 weeks, 4 weeks, and 17 weeks post AAV injection. After 17 weeks post AAV injection, 14 mice (7 males and 7 females) had serum cholesterol levels over 700mg/dL. At 18 weeks post AAV injection, the baseline group (4 mice, 3 females/1 male) was sacrificed; both aortic roots and arches were harvested as well as serum cholesterol to determine baseline levels of plaque and cholesterol. The remaining mice were separated into two groups, a control group switched to chow alone (4 mice, 2 females/2 males) and a treatment group switched to chow and treated with IL-4 (6 mice, 2 females/4 males). The treatment group was given 4 treatments of IL4-Fc (10µg per dose) for two weeks. After 2 weeks treatment and on the chow diet, which is 20 weeks post AAV injection, mice in the control group and the treatment group were sacrificed; both aortic roots and arches were harvested as well as serum cholesterol. After sectioning the aortic roots, and staining for CD68 plaque area, we observed a trend towards increase in plaque area in the IL-4 treatment group (Figure 3), which was the opposite of what we expected. One possibility is that IL-4 treatment expanded the population of M2

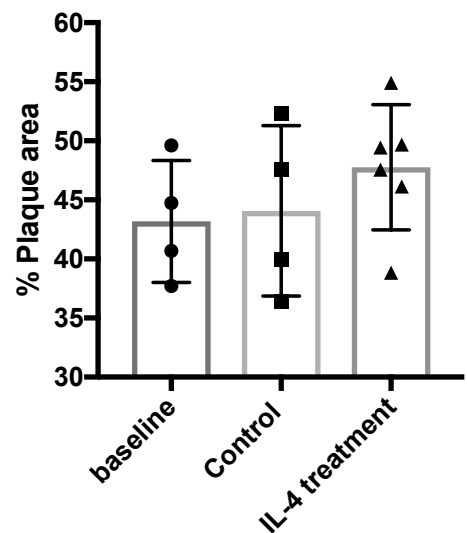


Fig. 3. IL-4-Fc treatment does not significantly alter plaque regression. AAV-PCSK9 treated mice were fed a Western Diet to induce plaques and then treated with 10 µg of IL-4-Fc for 2 weeks before sacrifice. Plaque area of aortic roots were measured and there is a trend towards greater plaque area in the IL-4 treated group, which was surprising since we expected IL-4 to enhance regression.

macrophages in the plaques, but have yet to begin the process of plaque resolution.

- Hence, to address the question of whether plaques need more time to remodel after IL-4 treatment, we performed a second experiment. In the second experiment, 15 *Cx3cr1*-Cre Rosa flox-tdTomato mice (5 females/10 males) were treated with an AAV expressing a hyper-active form of the PCSK9 gene and fed the mice on a Western Diet (WD). Serum cholesterol levels were monitored at 2 weeks, 4 weeks, 16 weeks and 19 weeks post AAV injection. At 19 weeks post AAV injection, 12 mice (5 females/7 males) were found to have serum cholesterol levels over 700mg/dL. At 20 weeks post AAV injection, mice were separated into two groups, a control group (6 mice, 3 females/3 males) and a IL-4 treatment group (6 mice, 2 females/4 males) for four weeks. The treatment group was switched to normal chow diet and given 4 treatments of IL4-Fc (10mg per dose) for the first two weeks, and then both groups stayed on the normal chow diet to enable time for plaque resolution. This study is ongoing and the mice will be sacrificed at 24 weeks post AAV injection, aortic roots and arches will be harvested and analyzed.

Major Task 5: Loke lab: Generate ATAC-seq data from monocyte derived M2 macrophages from atherosclerosis plaques.

- Although in principle, we should be able to generate ATAC-seq data from as few as 5000 tdTomato positive macrophages from the aorta, in practice, we have not been able to obtain sequencing libraries of sufficient quality from sorted cells. We typically obtain 2-4,000 cells per animal from our experiments, thus far our ATAC-seq libraries have failed with this small number of cells. Recently, there have been published improvements on the ATAC-seq technique for very small cell numbers and we are optimizing and practicing these new protocols. Our success in obtaining single-cell RNA seq results (see below) has shifted our focus slightly towards the interpretation of those results first.

Major Task 6: Fisher and Loke labs: Generate RNA-seq data from monocyte derived M2 macrophages from atherosclerosis plaques.

- Due to the recent availability of the 10X genomics platform for single cell RNA seq analysis, we have applied this approach towards characterizing the transcriptional profiles of monocyte derived macrophages in atherosclerosis progression and regression. We used a combination of single-cell RNA sequencing and genetic fate mapping approaches described above to profile 3157 and 2198 aortic cells derived from CX3CR1+ precursor in atherosclerotic mice during plaque progression and regression. These experiments revealed a spectrum of macrophage activation states with greater complexity than the traditional definition of M1 and M2 (Figure 4)

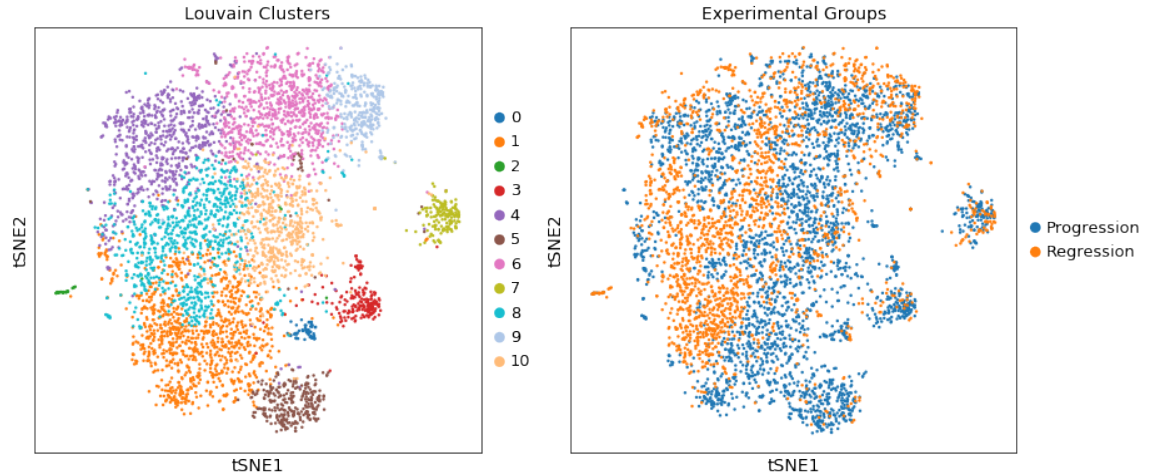


Fig. 4. Diversity of fate-mapped Mφs in progressing and regressing plaques. Mice under progression or regression conditions were injected with TAM and the TdTomato+ cells were sorted by FACS. Single cell libraries were prepared using the 10X Genomics system for RNA-seq. Normalized and aggregated data are displayed as a tSNE plot.

- From these data, we found that progression is associated with differentiation of monocytes into more distinct macrophage activation states than during regression. We also identified an unexpected cluster of proliferating monocytes with a stem cell like signature suggesting that monocytes may persist in a proliferating self-renewal state in inflamed tissue, rather than differentiate immediately into macrophages after entering the tissue.
- These data are currently being submitted for publication.

Major Task 7: Integrate ATAC-seq and RNA-seq data to build a transcriptional network for M2 activation in regressing plaques.

- We have not yet embarked on this Task since we have not been able to obtain ATAC-seq data of sufficient quality as yet, but are developing computational models to build a transcriptional network based on single-cell RNAseq results that we have already obtained from macrophages in progressing and regressing plaques.

Aim 2 Major Tasks:

Major Task 1: Fisher lab: Determine the efficacy of nanoparticles containing LXR agonist to promote plaque regression in LDLR^{-/-} mice.

- All of these studies were successfully completed in the first funding period.

Major Task 2: Fisher lab: Characterize changes to plaque macrophages after treatment with LXR-agonist-NP.

- All of these studies were successfully completed in the first funding period and has now been successfully published (see below).

Major Task 3: Moore lab: Determine the efficacy of nanoparticles containing Netrin1- and Unc5b-siRNA to promote plaque regression in LDLR-/- mice.

- We have completed a study to determine the effects of nanoparticles containing Unc5b-siRNA on aortic atherosclerosis in Ldlr-/- mice, as compared to empty nanoparticles. Surprisingly, we observed that empty nanoparticles alone were very effective at reducing plaque area in Ldlr-/-. Hence, the addition of the Unc5b-siRNA did not have a significant effect above the beneficial effect of the empty nanoparticles alone. One possibility is that the empty nano-particles have been previously shown to be effective at removing cholesterol from cells. We are currently investigating if this is indeed the case and have paused these studies until we understand the effects of the empty nanoparticles alone.

Major Task 4: Moore lab: Characterize changes to plaque macrophages after treatment with Netrin1- and Unc5b-siRNA -NP.

- This task will be undertaken after we understand the effects of the empty nanoparticles as part of Major Task 3.

What opportunities for training and professional development did the project provide?

Postdoctoral Fellows:

- **Dr. Jian-Da Lin, Ph.D.**, is an expert in immunology who has been working on this project and as a result is being trained in the field of atherosclerosis. His previous research experience was on inflammatory responses to viral infections in the gut, and he is applying this immunology expertise to the project while learning techniques specific for atherosclerosis.
- **Dr. Ada Weinstock, Ph.D.**, is also well trained in immunology, who through this grant, has been able to gain experience in atherosclerosis models. She has been able to use this experience to the IL4/IL13 component of Task 1a.
- **Milessa Afonso, Ph.D.**, is an expert in lipid metabolism, who through this grant, has gained experience in mouse models of atherosclerosis and its analysis.

Graduate Students: None trained under this grant.

5. CHANGES/PROBLEMS:

We have had challenges in the generation of quality ATAC-seq sequencing libraries from cells obtained from the aorta. We are still currently optimizing this process, but we are also exploring how to generate transcriptional networks with single-cell RNA-seq data, which we have already obtained.

6. PRODUCTS:

Yu M, Amengual J, Menon A, Kamaly N, Zhou F, Xu X, Saw PE, Lee SJ, Si K, Ortega CA, Choi WI, Lee IH, Bdour Y, Shi J, Mahmoudi M, Jon S, Fisher EA, Farokhzad OC. Targeted Nanotherapeutics Encapsulating Liver X Receptor Agonist GW3965 Enhance Antiatherogenic Effects without Adverse Effects on Hepatic Lipid Metabolism in Ldlr^{-/-} Mice. Adv Healthc Mater. 2017 Oct;6(20).

7. PARTICIPANTS & OTHER COLLABORATING ORGANIZATIONS:

Has there been a change in the active other support of the PD/PI(s) or senior/key personnel since the last reporting period?

Yes, Dr. Loke have changes in other support.

Loke, Png

Recently Funded

Title:	Interactions between helminth colonization and the gut microbiota
Time Commitment:	1.8 Cal Months
Supporting Agency:	NIAID
Grants Officer:	John T. Pesce
Performance Period:	01/01/2018 – 12/31/2022
Level of Funding:	\$ 433,103
Project Goals:	This project examines the effect of helminth infections in the Orang Asli populations in Malaysia by longitudinal analyses of samples before and after deworming treatment.
Specific Aims:	Aim 1: Determine if the effects of helminth colonization on the gut microbiota is dependent on prevalence and burden of helminth. Aim 2: Isolation and characterization of novel Clostridiales strains from the Orang Asli.
Overlap:	None

Recently Completed

Title:	Role of Nod2 in preventing intestinal disease downstream of microbial imbalances
Time Commitment:	1.2 Cal Months
Supporting Agency:	NIDDK
Grants Officer:	Peter J Perrin
Performance Period:	08/01/2015 – 07/31/2018
Level of Funding:	\$225,000
Project Goals:	The focus of this project is to investigate the inflammatory properties of the microbiota in Nod2 deficient mice and to determine how inflammatory responses can be reversed.
Specific Aims:	Aim 1. Determine if <i>B. vulgatus</i> directly causes intestinal abnormalities in Nod2 ^{-/-} mice. Aim 2. Characterize B cell deficiencies in Nod2 ^{-/-} mice and determine if this causes expansion of <i>B. vulgatus</i> . Aim 3. Determine the mechanism by which <i>T. muris</i> suppresses <i>B. vulgatus</i> in Nod2 ^{-/-} mice.
Overlap:	None

What other organizations were involved as partners?

Nothing to Report

8. SPECIAL REPORTING REQUIREMENTS:

COLLABORATIVE AWARDS: We have included a duplicative report for both the Initiating PI and the Collaborating/Partnering PI and noted the lab assignments to the different labs for the Major Tasks.

9 APPENDICES: see attached documents

Targeted Nanotherapeutics Encapsulating Liver X Receptor Agonist GW3965 Enhance Antiatherogenic Effects without Adverse Effects on Hepatic Lipid Metabolism in *Ldlr*^{-/-} Mice

Mikyung Yu, Jaume Amengual, Arjun Menon, Nazila Kamaly, Felix Zhou, Xiaoding Xu, Phei Er Saw, Seung-Joo Lee, Kevin Si, Carleena Angelica Ortega, Won Il Choi, In-Hyun Lee, Yazan Bdour, Jinjun Shi, Morteza Mahmoudi, Sangyong Jon, Edward A. Fisher,* and Omid C. Farokhzad*

The pharmacological manipulation of liver X receptors (LXRs) has been an attractive therapeutic strategy for atherosclerosis treatment as they control reverse cholesterol transport and inflammatory response. This study presents the development and efficacy of nanoparticles (NPs) incorporating the synthetic LXR agonist GW3965 (GW) in targeting atherosclerotic lesions. Collagen IV (Col IV) targeting ligands are employed to functionalize the NPs to improve targeting to the atherosclerotic plaque, and formulation parameters such as the length of the polyethylene glycol (PEG) coating molecules are systematically optimized. In vitro studies indicate that the GW-encapsulated NPs upregulate the LXR target genes and downregulate proinflammatory mediator in macrophages. The Col IV-targeted NPs encapsulating GW (Col IV–GW–NPs) successfully reaches atherosclerotic lesions when administered for 5 weeks to mice with preexisting lesions, substantially reducing macrophage content (≈30%) compared to the PBS group, which is with greater efficacy versus nontargeting NPs encapsulating GW (GW–NPs) (≈18%). In addition, mice administered the Col IV–GW–NPs do not demonstrate increased hepatic lipid biosynthesis or hyperlipidemia during the treatment period, unlike mice injected with the free GW. These findings suggest a new form of LXR-based therapeutics capable of enhanced delivery of the LXR agonist to atherosclerotic lesions without altering hepatic lipid metabolism.

1. Introduction

Atherosclerosis is the most common cause of coronary artery disease, which accounts for the largest number of deaths in the United States. This pathology is characterized by deposition of cholesterol and triglyceride (TG)-rich lipoproteins within the arterial wall, leading to an inflammatory response. Consequently, circulating monocytes are recruited into the arterial wall and undergo differentiation into macrophages, which can progressively transform into cholesterol-laden foam cells. The continuous accumulation of foam cells and extracellular materials generates the atherosclerotic plaques that can rupture and cause acute local occlusive thrombosis, and this eventually results in myocardial infarction or stroke.^[1]

Liver X receptors (LXR α and LXR β) are a family of nuclear receptors that control the expression of key proteins regulating lipid metabolism by dimerizing with retinoid X receptors (RXRs).^[2] In

Dr. M. Yu, Dr. N. Kamaly, Dr. X. Xu, Dr. P. E. Saw, K. Si, C. A. Ortega, Dr. W. I. Choi, Dr. I.-H. Lee, Y. Bdour, Dr. J. Shi, Dr. M. Mahmoudi, Prof. O. C. Farokhzad
Center for Nanomedicine and Department of Anesthesiology
Brigham and Women's Hospital
Harvard Medical School
Boston, MA 02115, USA
E-mail: ofarokhzad@bwh.harvard.edu

Dr. J. Amengual, Dr. A. Menon, F. Zhou, Prof. E. A. Fisher
Division of Cardiology
Department of Medicine
Marc and Ruti Bell Program in Vascular Biology
New York University School of Medicine
New York, NY 10016, USA
E-mail: edward.fisher@nyumc.org
Dr. N. Kamaly
Department of Micro and Nanotechnology
Technical University of Denmark
DTU Nanotech
2800 Kgs. Lyngby, Denmark


DOI: 10.1002/adhm.201700313

Dr. S.-J. Lee
Department of Biological Chemistry and Molecular Pharmacology
Harvard Medical School
240 Longwood Ave., Boston, MA 02115, USA

Dr. W. I. Choi
Center for Convergence Bioceramic Materials
Convergence R&D Division
Korea Institute of Ceramic Engineering and Technology
202, Osongsaengmyeong 1-ro, Osong-eup, Heungdeok-gu
Cheongju, Chungbuk 28160, Republic of Korea

Dr. S. Jon
KAIST Institute for the BioCentury
Department of Biological Sciences
Korea Advanced Institute of Science and Technology (KAIST)
291 Daehak-ro, Daejeon 34141, Republic of Korea

Prof. O. C. Farokhzad
College of Pharmacy
King Abdulaziz University
Jeddah 21589, Saudi Arabia

 The ORCID identification number(s) for the author(s) of this article can be found under <https://doi.org/10.1002/adhm.201700313>.

macrophages, LXR activation increases the expression of the cholesterol transporter ATP-binding cassette transporter sub-families A member 1 (ABCA1) and G member 1 (ABCG1), promoting cholesterol efflux to apolipoprotein A1 (ApoA1) and high-density lipoprotein (HDL), respectively, which transport cholesterol to the liver for further elimination. LXR activation also dampens the gene expression of proinflammatory genes by various mechanisms including SUMOylation-mediated transrepression and histone acetylation modification, among others.^[3] Hence, synthetic LXR agonists such as GW3965 (referred to as GW) simultaneously promote cholesterol efflux and hamper pro-inflammatory signals in plaque macrophages, offering a seemingly attractive pharmacological alternative to treat atherosclerosis. Unfortunately, their beneficial effects on atherosclerosis are accompanied by an undesirable increase in plasma levels and hepatic content of lipids, particularly TG, which has hindered Food and Drug Administration (FDA) approval of the LXR agonists that have entered clinical trials.^[4–6] Therefore, innovative strategies that reduce the adverse side effects of LXR activation while maintaining efficacy, such as tissue-selective LXR-based therapeutics, are needed.

Nanomedicines have shown successful patient outcomes in clinical trials by improving the pharmacokinetic profile of cytotoxic drugs and decreasing their toxicity.^[7–9] Nanoparticles (NPs) designed to accumulate in desired tissues, the next generation of NP-based therapies, are also currently in clinical trials.^[10,11] While targeted NPs have been thoroughly investigated for cancer treatment, only a few studies of nanotherapeutics actively targeting atherosclerosis have been reported (e.g.,^[12,13]). Our group previously developed polymeric NPs encapsulating GW to enhance the proresolving activity and mitigate the toxicity of GW.^[14,15] Those strategies, however, did not include a systematic method for the formulation and optimization of targeted nanoplateforms in the treatment of inflammatory diseases. Herein, we report the development of NPs encapsulating GW designed to have selective advantage in targeting atherosclerotic lesions over the liver, and their therapeutic efficacy in the *Ldlr*^{−/−} mouse model of atherosclerosis. We chose a collagen IV (Col IV)-targeting heptapeptide ligand identified previously by our group,^[16] to deliver our NP formulation to atherosclerotic lesions, as the Col IV-targeted NPs previously developed for the delivery of peptide Ac2-26 and IL-10 to plaques exhibited superior targeting abilities to nontargeting NPs via the specific binding with Col IVs overexpressed at sites of atherosclerosis.^[17–19]

The NPs in this study comprise three distinct functional components: (i) a biodegradable hydrophobic polymeric core (poly(D,L-lactide) (PLA) with terminal ester groups); (ii) a lipid layer of methoxy(polyethylene glycol) (mPEG)-functionalized phospholipids and 1,2-dilauroyl-sn-glycero-3-phosphocholine (DLPC); and, (iii) a Col IV targeting peptide conjugated to a 1,2-distearoyl-sn-glycero-3-phosphoethanolamine (DSPE)-PEG with a molecular weight of 2000 kDa (Col IV–DSPE–PEG2000 conjugate) as part of the surface layer. The lipid–polymer hybrid NPs have been reported as promising platforms for small-molecule drug delivery,^[20] protein delivery,^[21] and gene delivery^[22] owing to the complementary characteristics of polymeric NPs and liposomes that enhance their physical stability and biocompatibility. To obtain ideal targeted NPs for in vivo

use, optimization of the weight ratio of polymer to lipids, the molar ratio of the lipids making up the surface layer, and the length of the PEG-coating molecules on the surface of the NPs are all critical. Here, we report the results of the systematic optimization of the formulation parameters above to construct the Col IV-targeting NPs and their GW encapsulation. Notably, we demonstrate that these NPs have antiatherogenic effects on macrophages in vivo without altering plasma or hepatic lipid homeostasis. This new targeted NP system for the delivery of GW to atherosclerotic plaques suggests a new modality for combating inflammation in advanced atherosclerosis.

2. Results and Discussion

2.1. Formulation Parameters of PLA–DSPE–mPEGs–DLPC–NPs

PEGylation has been a key process in reducing the formation of protein corona on the surface of NPs, which can hinder the recognition of their receptor targets in the blood stream. PEG is a promising antifouling polymer for use in engineering NPs. However, it is also important to choose the right density and length of the PEG-coating molecules in designing targeted NPs with optimal binding specificity, as PEG interferes with the binding of the targeting ligand to its target.^[23] The biorecognition of targeted liposomes and inorganic NPs was maximized when the length of the PEG-coating molecules was properly shortened relative to the ligand linker.^[23–26] On the other hand, the optimal length of targeted lipid–polymer hybrid NPs was not yet been identified. To examine the effects of the length of PEG-coating molecules on lipid–polymer NPs, a series of NPs with various lengths of methoxy-capped PEGylated phospholipids (DSPE–mPEGs) with diverse molecular weights (DSPE–mPEG550, DSPE–mPEG1000, and DSPE–mPEG2000) were prepared using a modified emulsion method (Figure 1A). An organic phase mixture with an 80:20 (v/v) ratio of ethyl acetate and benzyl alcohol was used to solubilize the lipids (DSPE–mPEGs and DLPC) as well as the ester-terminated PLA (PLA–OCH₃) prior to rapid mixing with the aqueous phase. After overnight evaporation of the organic solvents, self-assembled NPs consisting of a hydrophobic polymer core (PLA–OCH₃) surrounded by a lipid layer of DLPC/DSPE–mPEG550, DLPC/DSPE–mPEG1000 or DLPC/DSPE–mPEG2000 were obtained: NPs(550), NPs(1000), and NPs(2000), respectively. Our studies revealed that all lipids could be simply dissolved in an organic phase in which polymers were solubilized without an additional heating step that was frequently needed to dissolve the lipids in the aqueous phase previously.^[27,28]

To investigate the effects of the molar ratio of lipid–PEG/lipid (DSPE–mPEGs/DLPC)-containing lipid layer and the weight ratio of total lipids/polymer (DSPE–mPEGs + DLPC/PLA–OCH₃) on NP size, lipid–PEG/lipid molar ratios of 1:9, 3:7, 7:3, and 10:0 were tested against total lipids/polymer weight ratios of 0.5:1, 0.7:1, and 1:1. In all formulations of NPs(550), NPs(1000), and NPs(2000), increasing the total lipids/polymer weight ratio yielded smaller NPs (Figure 1B). At the total lipids/polymer weight ratio of 0.5:1, an increase in lipid–PEG/lipid molar ratio from 1:9 to 10:0 did not alter NP size, whereas an increase in the lipid–PEG/lipid molar

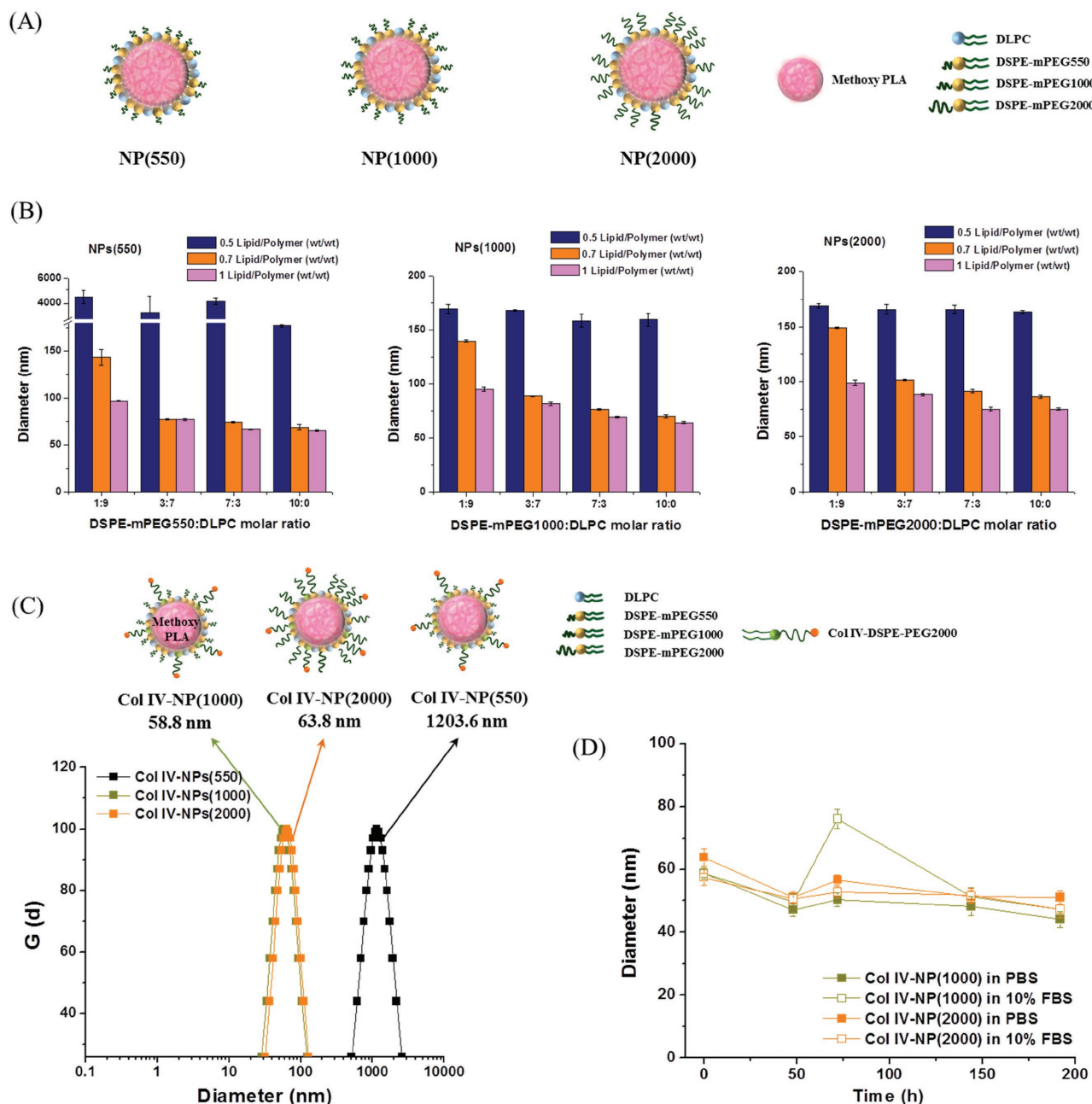


Figure 1. Development of the lipid–polymer hybrid NPs with various lengths of methoxy-capped PEGylated phospholipids (DSPE–mPEGs) with diverse molecular weights (DSPE–mPEG550, DSPE–mPEG1000, and DSPE–mPEG2000), and engineering of the Col IV–targeting NPs. A) Schematics of the NP(550), NP(1000), and NP(2000) comprising PLA cores surrounded by DLPC/DSPE–mPEG550, DLPC/DSPE–mPEG1000, and DLPC/DSPE–mPEG2000, respectively. B) NPs(550), NPs(1000), and NPs(2000) with variations in the formulation parameters such as weight ratio of total lipids to PLA (0.5, 0.7, and 1, wt/wt) and molar ratio of DSPE–mPEGs to DLPC (1:9, 3:7, 7:3, and 10:0) were measured by DLS in distilled water. C) Hydrodynamic size measurement of the Col IV–NPs in PBS using DLS. Col IV–NPs(550), Col IV–NPs(1000), and Col IV–NPs(2000) were synthesized with DSPE–mPEGs, DLPC, and Col IV–DSPE–PEG2000 (67.5:27.5:5, molar ratio) at 70% of the PLA weight. DSPE–mPEG550, DSPE–mPEG1000, and DSPE–mPEG2000 were used for the preparation of Col IV–NPs(550), Col IV–NPs(1000), and Col IV–NPs(2000), respectively. D) In vitro stabilities of Col IV–NPs in PBS and 10% FBS at 37 °C. Data are expressed as mean \pm SEM.

ratio from 1:9 to 3:7 substantially reduced the NP size at total lipids/polymer weight ratios of 0.7:1 and 1:1. The results indicate that NP sizes can be finely tuned given the presence of sufficient amounts of total lipids covering the hydrophobic PLA core. We chose formulations with diameters <100 nm in

distilled water as suitable for further modification and characterization. Thus, a total lipids/polymer weight ratio of 0.7:1 and a lipid–PEG/lipid molar ratio of 3:7 were considered minimum requirements for optimal NP formulation with minimal PEG content.

Next, we examined the stability of the NPs over time by monitoring changes in their size. We incubated NPs(550), NPs(1000), and NPs(2000) with a total lipids/polymer weight ratio of 0.7:1 and lipid-PEG/lipid molar ratios of 3:7 or 7:3 in PBS and PBS containing 10% fetal bovine serum (FBS) at 37 °C. As shown in Figure S1 (Supporting Information), most of the NPs were stable in both solutions for 7 d, maintaining their size between 35 and 45 nm. Particularly, the hydrodynamic sizes of the NPs in PBS and PBS containing 10% FBS were slightly smaller than those measured in distilled water because of the increased ionic strength on the surface of NPs in PBS solution.^[29] In contrast, NPs(550) with a lipid-PEG/lipid molar ratio of 3:7 significantly increased in size in PBS containing 10% FBS within 2 d, suggesting that the higher density of PEG-coating molecules is required to achieve stealth function when they are short in length. Hence, a lipid-PEG/lipid molar ratio of 7:3 was selected as the final formulation parameter for further modification of the NPs(550), NPs(1000), and NPs(2000).

2.2. Preparation of Col IV-NPs with Various PEG Lengths

The length of PEG used for conjugating with Col IV targeting ligand was fixed by selecting a DSPE-PEG with molecular weight of 2000 kDa, since it was the most commonly used in developing targeted lipid-polymer hybrid NPs.^[30–32] To engineer Col IV-targeting lipid-polymer NPs (Col IV-NPs) with various lengths of PEG-coating molecules, the Col IV-DSPE-PEG2000 conjugate was first synthesized by conjugating the KLWVLPK peptide to maleimide-functionalized DSPE-PEG2000 (DSPE-PEG-MAL) via the free thiol of the C-terminal GGGC linker using maleimide chemistry, and purified by HPLC. MALDI TOF results indicate that the DSPE-PEG-MAL (average MW: 2941.6 Da) was conjugated to the peptide (MW: 1157.4 Da), yielding a Col IV-DSPE-PEG2000 conjugate (average MW: 4076.9 Da), which was successfully purified (Figure S2, Supporting Information). Multiple peaks in the MALDI results are attributable to the polydispersity of PEG. Next, a series of Col IV-NPs, i.e., Col IV-NPs(550), Col IV-NPs(1000), and Col IV-NPs(2000), were prepared by pairing the Col IV-DSPE-PEG2000 with DSPE-mPEG550/DLPC, mPEG1000/DLPC, and mPEG2000/DLPC. As shown in Figure 1C, the hydrodynamic sizes of the Col IV-NPs(1000) and Col IV-NPs(2000) were 58.8 ± 0.6 and 63.8 ± 0.7 nm, respectively. Whereas, Col IV-NPs(550) was larger than ≈ 1 μ m, indicating that at least PEG1000 is needed for stabilizing the Col IV-targeting ligand-modified surface as well as successful coating of the NPs. The hydrodynamic sizes of Col IV-NPs(1000) and Col IV-NPs(2000) were stable throughout the 192 h study in both PBS and PBS containing 10% FBS (Figure 1D).

Binding studies for the Col IV-NPs were then performed via SPR measurement. The NPs(1000) and NPs(2000) were employed as control NPs to demonstrate the targeting abilities of Col IV-targeting peptides decorated on the Col IV-NPs(1000) and Col IV-NPs(2000), respectively. We found that the Col IV-NPs(1000) specifically bound to Col IV proteins even at a low concentration (0.3 mg mL⁻¹) and remained on

the Col IV surface with no appreciable dissociation owing to the multivalent interactions of the NPs (Figure S3A, Supporting Information).^[33] In contrast, no binding was observed in Col IV-NPs(2000), in which the length of the PEG-coating molecules (DSPE-mPEG2000) used to construct the NPs was similar to that of the targeting ligand displaying lipid-PEG (Col IV-DSPE-PEG2000), as well as in nontargeting NPs(1000) and NPs(2000) (Figure S3B–D, Supporting Information). These results suggest that the PEG conjugated with the Col IV targeting ligand should be longer than the PEG coated on the surface of lipid-polymer hybrid NPs, similar to the PEGylated liposomal or inorganic targeted NPs.^[23,26] Consequently, the Col IV-NPs(1000) surrounded by a lipid layer of DSPE-mPEG1000/DLPC/Col IV-DSPE-PEG2000 were considered optimal and suitable for further use in cell culture and in vivo studies. The optimized NPs(1000) and Col IV-NPs(1000) maintained their size between 41 and 64 nm in serum (100% FBS) for 48 h without generating aggregates (Figure S4, Supporting Information).

2.3. Synthesis and Characterization of GW-Encapsulated Col IV-NPs (Col IV-GW-NPs)

Next, GW was encapsulated into the Col IV-NPs through the modified emulsion method (Figure 2A). A nanoemulsion process using GW in an organic phase mixture and a formulation of 0.7:1 of total lipids/polymer weight ratio, 67.5:27.5:5 of DSPE-mPEG1000/DLPC/Col IV-DSPE-PEG2000 molar ratio, and 0.26–0.54 dL/g PLA-OCH₃ polymer inherent viscosity core yielded Col IV-GW-NPs with a drug loading amount of 10.8 wt% (encapsulation efficiency/EE: 45%). Likewise, empty NPs (which have no drug) and nontargeting GW-NPs were prepared. The loading amount of GW in the GW-NPs was 12.0 wt% (EE: 57%). The GW loading amounts (10.8–12.0 wt%) in the lipid-polymer hybrid NPs were comparable to or higher than the previously developed GW-encapsulated polymeric NPs (2.5–10.9 wt%), whereas their hydrodynamic sizes were smaller than the previous ones (100–156 nm). The hydrodynamic sizes of the empty NPs, GW-NPs, and Col IV-GW-NPs in PBS were 41.9 ± 0.4 , 73.8 ± 1.3 , and 83.9 ± 2.6 nm, respectively (Figure 2B). The increase in the hydrodynamic sizes of GW-NPs and Col IV-GW-NPs implies successful drug encapsulation and functionalization with Col IV targeting ligands. To demonstrate their colloidal stability in serum, we dispersed the NPs in serum (100% FBS) and measured them. The hydrodynamic sizes of the empty NPs, GW-NPs, and Col IV-GW-NPs in serum were 41.1 ± 0.5 , 80.3 ± 3.5 , and 86.7 ± 1.2 nm, respectively (Figure 2B), indicating negligible or little increase in their size due to protein corona formation. These results demonstrate the high colloidal stability of the stealth-like NPs even in the presence of serum proteins.^[34] Additionally, we performed nanoparticle tracking analysis (NTA) for the NPs, GW-NPs, and Col IV-GW-NPs, and the hydrodynamic sizes of the groups were 77.0 ± 0.5 , 89.7 ± 0.4 , and 99.0 ± 1.4 nm, respectively, indicating a size increase trend similar to that observed in dynamic light scattering (DLS) (Figure S5, Supporting Information).

These results show that the modified emulsion method yielded small-sized lipid-polymer hybrid NPs with a higher

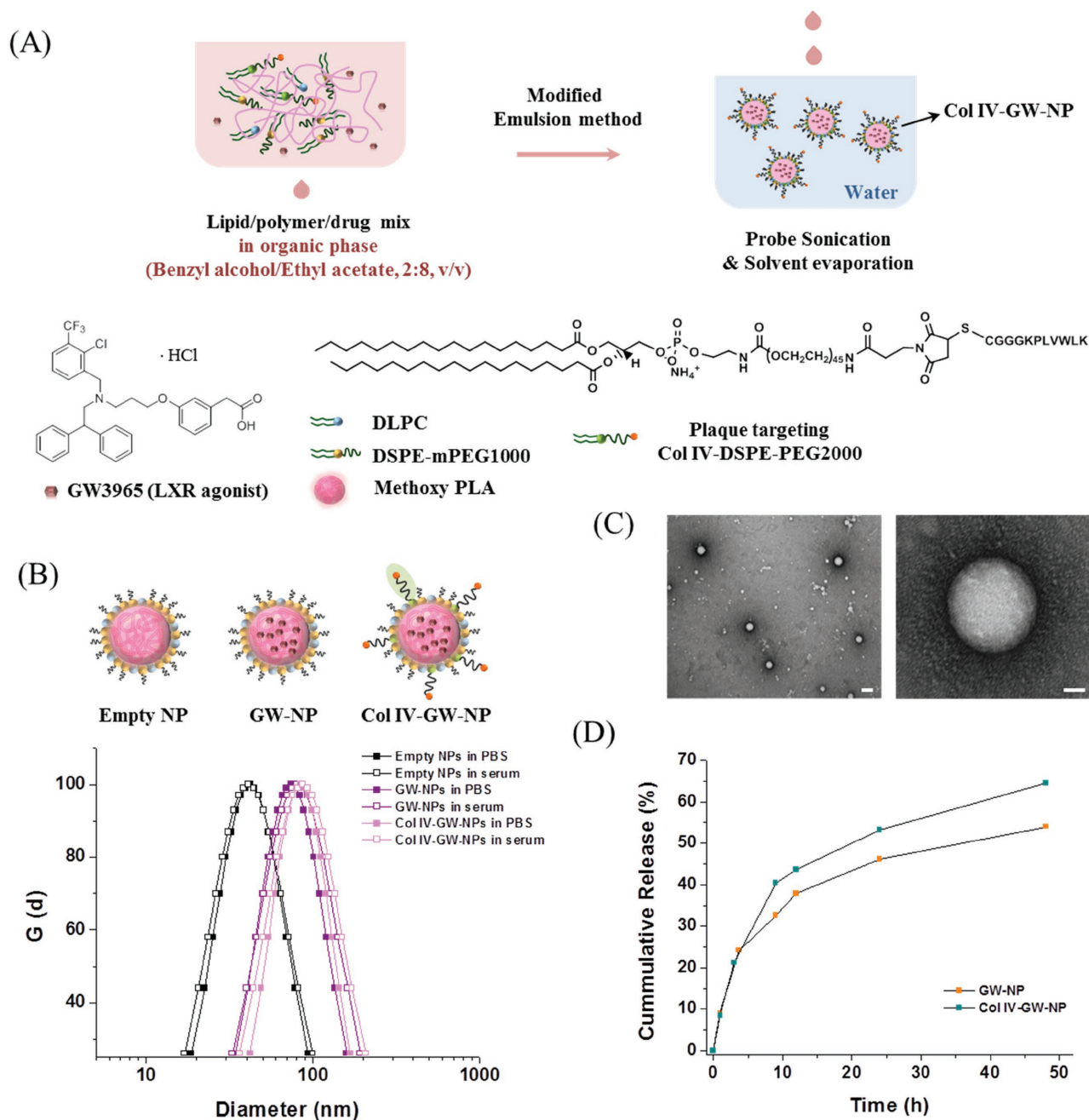


Figure 2. Formulation and characterization of GW-encapsulated NPs. A) Schematic of Col IV-GW-NP design. The lipids/polymer/drug mixture were dissolved in benzyl alcohol/ethyl acetate co-solvent (2:8, v/v), and the NPs were formed by modified single-emulsion method in water via a single self-assembly process. B) The mean hydrodynamic diameters of empty NPs, GW-NPs, and Col IV-GW-NPs in PBS and serum (100% FBS), respectively, determined by DLS. C) Representative TEM images of Col IV-GW-NPs. The scale bars of the left image and the right high-magnification image are 100 and 20 nm, respectively. D) In vitro drug release profiles of GW-NPs and Col IV-GW-NPs incubated at 100 rpm and 37 °C in PBS.

drug-loading capacity compared to nanoprecipitation or previous emulsion methods using polyvinyl alcohol. The surface charges of the empty NPs, GW-NPs, and Col IV-GW-NPs were -11.4 ± 4.1 , -4.4 ± 3.1 , and 1.8 ± 0.8 mV, respectively. Since the ends of the Col IV targeting peptide ligands have positively charged lysine groups, the surface charge of the GW-NPs was increased after the modification with Col IV targeting ligands. Transmission electron microscopy (TEM)

images revealed that the encapsulation of GW did not cause morphological changes, and the NPs were homogeneously dispersed in aqueous solution with a well-defined spherical shape (Figure S6, Supporting Information and Figure 2C). The size ranges of the empty NPs, GW-NPs, and Col IV-GW-NPs shown in TEM were 35–40, 60–75, and 65–85 nm, respectively, indicating similar trend observed in DLS results. The DLS and TEM results indicated that the drug loading did not generate

any aggregated precipitates, as the GW was evenly distributed by encapsulation throughout the hydrophobic core of the NPs.

Release kinetics studies of GW were then performed by incubating NPs in PBS at 37 °C and measuring the remaining GW concentrations in the NPs at different time intervals using HPLC. The cumulative release curves of the GW-NPs and Col IV-GW-NPs exhibit an initial fast release of GW ($\approx 23\%$) for the first ≈ 3.5 h, followed by sustained release, indicating half-lives of ≈ 40 and ≈ 23 h, respectively (Figure 2D). The incorporation of a 5% molar ratio of Col IV-DSPE-PEG2000 onto the lipid layer of the NPs slightly accelerated the rate of drug release. The GW release kinetics was similar to the release graphs of hydrophobic small-molecule drugs from previously developed lipid-polymer hybrid NPs,^[20] suggesting that shorter PEG-coating molecules (DSPE-mPEG1000) covering the surface of NPs did not significantly alter the drug release profile.

2.4. Col IV-GW-NPs Efficiently Deliver GW to Primary Cultured Macrophages

Next, we evaluated whether the GW, either encapsulated in the NPs (GW-NPs or Col IV-GW-NPs) or dissolved directly in the medium (free GW), could stimulate the LXRs in primary cultured macrophages and control transcription of several genes involved in the cholesterol efflux pathway, including ABCA1.^[35,36] We first assessed the uptake of the rhodamine-labeled NPs and Col IV-NPs in murine thioglycollate-elicited peritoneal macrophages. Confocal images and quantification results demonstrated comparable uptake of both NPs by macrophages (Figure 3A,B). We then evaluated the cellular internalization of the NPs and Col IV-NPs in the presence of different inhibitors such as filipin and chlorpromazine (CPZ), which represent caveolae- and clathrin-mediated endocytic pathways, respectively, or cytochalasin D

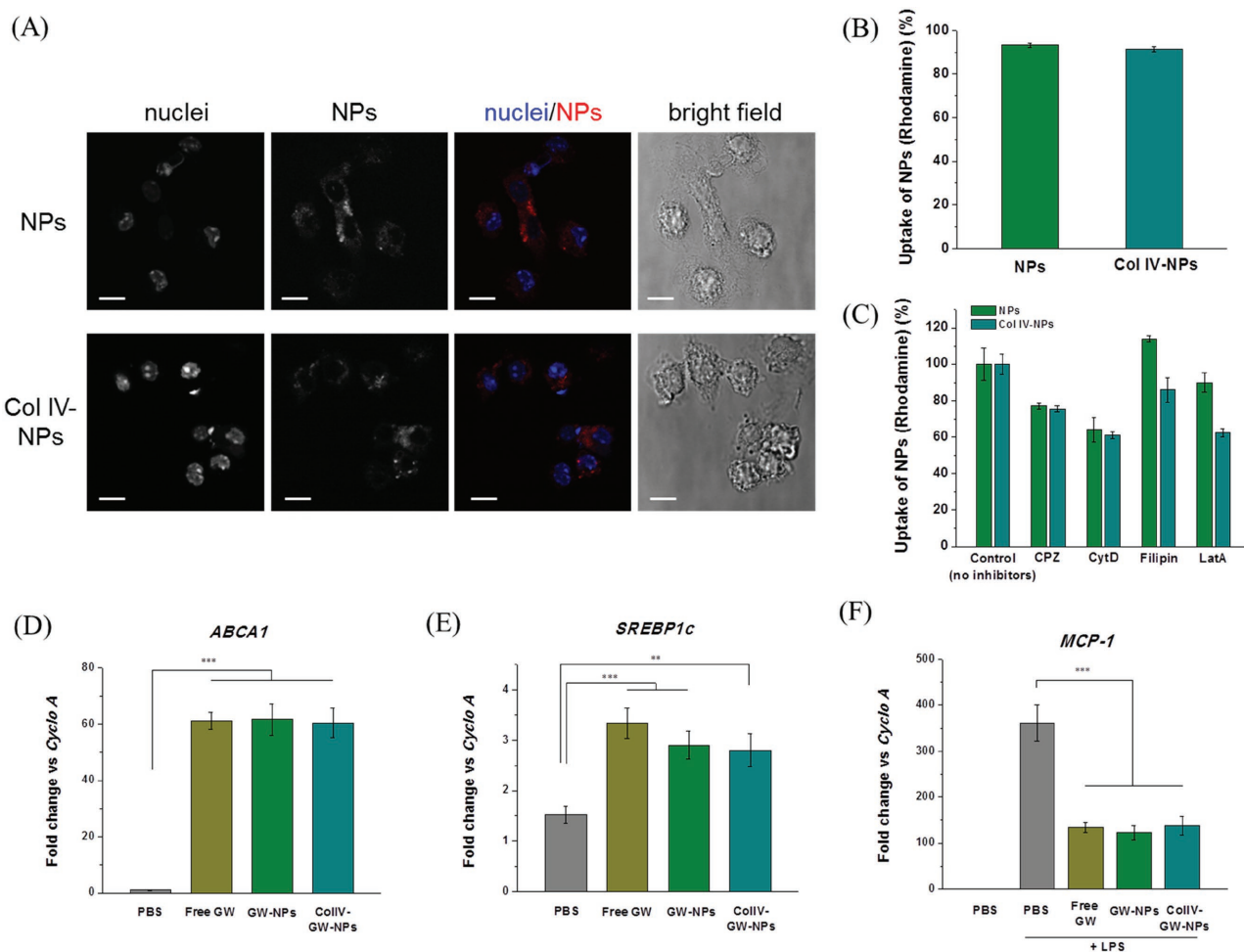


Figure 3. Effects of GW-NPs or Col IV-GW-NPs on LXR target gene expression in in vitro macrophages. To determine the uptake of the NPs, murine thioglycollate-elicited peritoneal macrophages were exposed to rhodamine-labeled NPs or Col IV-NPs for 4 h. A) Confocal microscopy shows the internalization of the NPs (red) into macrophages. Nuclei are represented in blue. Individual images are represented in grayscale. Cell shape is shown using the bright field. White bar; 10 μm . B) Quantification of the NPs uptake by macrophages using flow cytometry. C) NPs uptake in the presence of specific endocytic or phagocytic inhibitors. D,E) Murine thioglycollate-elicited peritoneal macrophages were exposed to the indicated treatments for 18 h at a concentration equivalent to 1×10^{-6} M of GW. F) After this period, cells were exposed to 100 ng mL⁻¹ of LPS for 6 h. After treatment, RNA was isolated and gene expression was analyzed by qRT-PCR. Cyclophilin A (Cyclo A) was used as housekeeping control. Experiments were performed in triplicate. (**p < 0.01 and ***p < 0.001). Data are expressed as mean \pm SEM.

(CytD) and Latrunculin A (LatA), which represent phagocytosis pathway. We observed $\approx 25\%$, $\approx 35\text{--}40\%$, and $\approx 10\text{--}38\%$ reductions of both NPs uptake upon treatment with CPZ, CytD, and LatA, respectively, suggesting the role of clathrin-mediated endocytosis and phagocytosis in both NPs uptake (Figure 3C). Then, we isolated thioglycollate-elicited macrophages from wild-type mice and exposed them to 1×10^{-6} M of free GW or equivalent GW dose of GW-NPs and Col IV-GW-NPs, respectively. After the corresponding treatments for 18 h, we isolated total mRNA from the treated macrophages and investigated the expression levels of two classical LXR target genes: ABCA1 and sterol regulatory element-binding transcription factor 1c (SREBP-1c). Notably, cells treated with the GW-NPs and Col IV-GW-NPs revealed markedly elevated mRNA levels of ABCA1 compared to those treated with PBS, which were used as a negative control (Figure 3D). These results were comparable to the findings in cells treated with free GW, demonstrating that GW-NPs and Col IV-GW-NPs efficiently delivered GW to macrophages and activated LXR signaling to a similar extent as did free GW. Following the same trend, the expression of SREBP1c was also increased by all the GW treatments (Figure 3E), indicating that LXR target genes were activated through the treatments with GW-NPs or Col IV-GW-NPs as well as with free GW.

In addition to the beneficial effects of LXR activation on cholesterol efflux, LXR signaling mediates potent anti-inflammatory effects.^[3] One of the best-characterized mechanisms is the transrepression of the Toll-like receptor 4 (TLR4) – lipopolysaccharide (LPS) signaling pathway, which is mediated by SUMOylation of the LXR receptor.^[4] Recently, upregulation of ABCA1 also revealed anti-inflammation as a critical mediator.^[37] To evaluate whether the GW-NPs or Col IV-GW-NPs could repress inflammatory gene expression in macrophages, we preincubated peritoneal macrophages for 18 h with 1×10^{-6} M of free GW, GW-NPs, or Col IV-GW-NPs, followed by stimulation with 100 ng mL^{-1} of LPS for 6 h. After the treatments, we isolated total mRNA from the treated macrophages and examined gene expression of the proinflammatory marker, monocyte chemoattractant protein-1 (MCP-1). As shown in Figure 3F, LPS stimulation substantially increased the mRNA levels of MCP-1 in cultured macrophages. In contrast, preincubation with free GW, GW-NPs, or Col IV-GW-NPs elicited significantly more trans-repression of MCP-1 expression compared to LPS treatment alone. Consistent with the observation in the LXR target gene expressions, our findings indicate that mRNA levels of MCP-1 in the cells treated with free GW and GW encapsulated in the NPs (GW-NPs or Col IV-GW-NPs) were similar, suggesting that the NPs successfully release the encapsulated drug molecules in cultured macrophages (as also shown in the in vitro GW release results), causing LXR activation of the macrophages and mediating anti-inflammation. Microscopic visualization after incubation with the aforementioned treatments, together with the measurement of lactate dehydrogenase (LDH) levels in the medium, exhibited that any experimental condition had a significant effect on cellular viability (data not shown).

2.5. Col IV-GW-NPs Treatment Promotes a Decrease in CD68+ Cells in Atherosclerotic Lesions

We next assessed the drug delivery capability of Col IV-GW-NPs to in vivo target atherosclerotic plaques, and compared it to that of GW-NPs. To monitor the GW and NPs in the *Ldlr*^{-/-} mouse model of atherosclerosis, we labeled GW with BODIPY (GW-BODIPY) (Figure S7, Supporting Information) and encapsulated it in the NPs or Col IV-NPs, in which the core of the NPs were labeled by incorporating the fluorescent polymer Cy5.5-conjugated PLA (PLA-Cy5.5) (Figure 4A). The resulting GW-BODIPY encapsulated NPs (GW-BODIPY-NPs) and Col IV-NPs (Col IV-GW-BODIPY-NPs) were injected into *Ldlr*^{-/-} mice fed a western diet for 14 weeks (8 mg of GW-BODIPY kg^{-1} for the NPs). We then sacrificed mice 4 h postinjection and collected the descending aortas, livers, and plasma to quantify the GW-BODIPY and PLA-Cy5.5 in tissues using the IVIS 200 in vivo imaging system.

Quantitative assessment of the aorta-to-liver fluorescent ratios and plasma fluorescence intensity in the mice revealed that both GW-BODIPY and PLA-Cy5.5 preferentially accumulated in the aortas of mice treated with the Col IV-GW-BODIPY-NPs to a greater extent than mice that received GW-BODIPY-NPs (Figure 4B and Figure S8, Supporting Information). However, the amounts of GW-BODIPY and PLA-Cy5.5 in plasma remained relatively unaltered in both groups (Figure 4C). These results indicate that the presence of the Col IV-targeting peptides on the surface of the NPs enhanced the delivery capability of GW to atherosclerotic lesions compared to the nontargeting NPs.

We next tested the relative benefits of Col IV-GW-NPs on atherosclerosis. For this purpose, *Ldlr*^{-/-} mice fed a western diet for 14 weeks to develop advanced atherosclerosis lesions were switched to a chow diet and injected intravenously with free GW, GW-NPs, or Col IV-GW-NPs (8 mg of GW kg^{-1} based on the amount of free GW) twice a week for 5 weeks (Figure 4D). As a control, another group of mice were injected with equal volumes of PBS. After the treatment period, mice were sacrificed and aortic roots were harvested to measure the plaque macrophage (CD68+ cells) content in the atherosclerotic lesion area, which reflects local inflammation known to contribute to atherosclerotic disease progression in both mice and humans.^[38] While treatment with free GW and GW-NPs elicited no decrease in CD68+ cells in the aortic lesion, mice treated with Col IV-GW-NPs had significantly reduced macrophage (CD68+ cell) content ($\approx 30\%$) compared to the PBS group, which was with greater efficacy versus GW-NPs ($\approx 18\%$) (Figure 4E,F). These and the fluorescent accumulation (Figure 4B) results argue that the Col IV-targeting peptides employed on the surface of the NPs led to more efficient delivery of GW to atherosclerotic plaques compared to the non-targeting GW-NPs or free GW, subsequently reversing inflammation in the atherosclerotic mice.

To evaluate the phenotypic alterations in the lesional plaque macrophages treated with free GW, GW-NPs, and Col IV-GW-NPs, we performed laser capture microdissection (LCM) on CD68+ areas, isolated total mRNA from the macrophages, and quantified gene expression via RT-PCR. We found an upregulated mRNA level of ABCA1 in the CD68+ macrophages of the mice treated with Col IV-GW-NPs compared to other treatment groups,

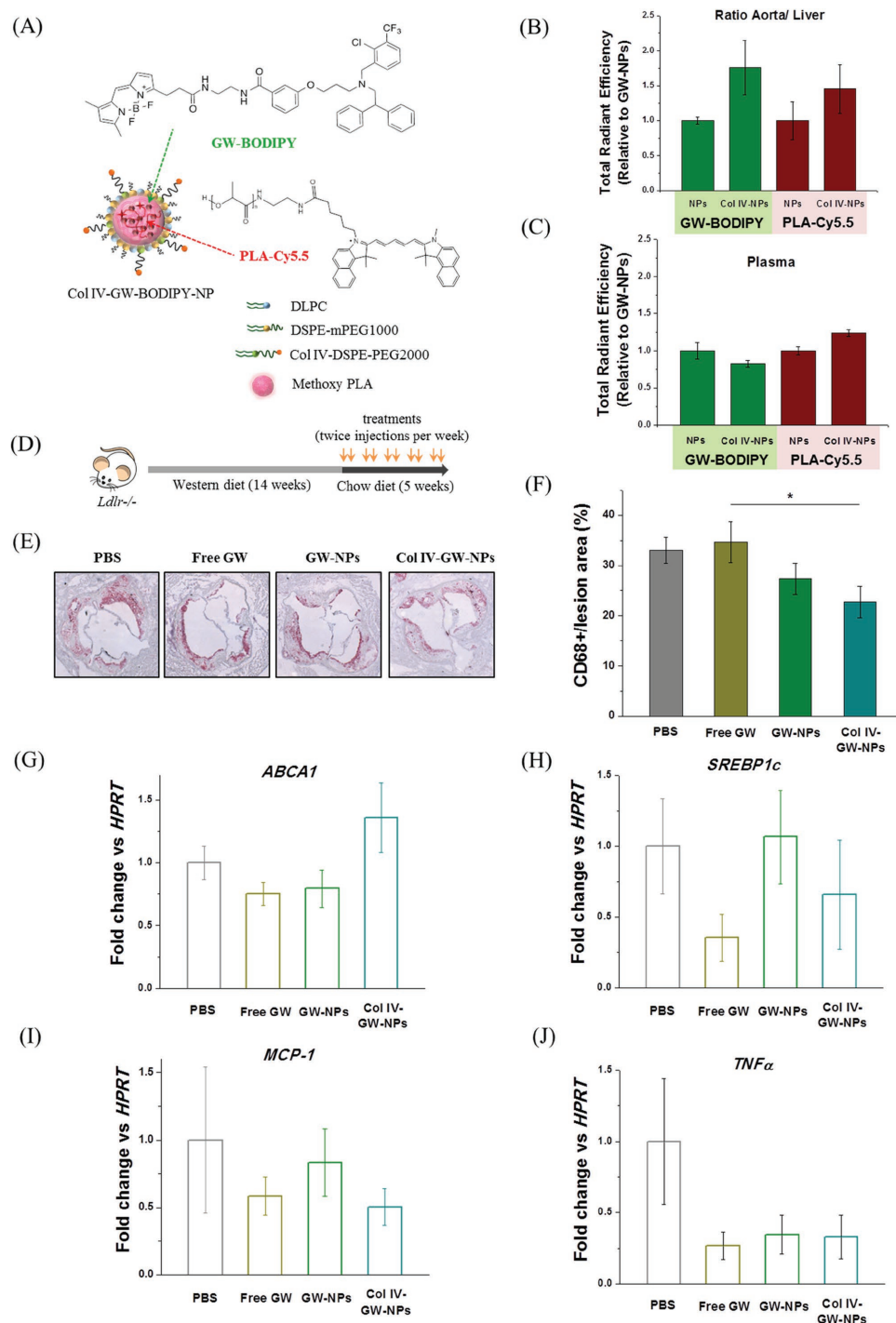


Figure 4. Plaque-targeting abilities and therapeutic efficacies of GW-NPs and Col IV-GW-NPs in the *Ldlr*^{-/-} mouse model of atherosclerosis. A) Schematic of the fluorescently labeled Col IV-targeting NP. Fluorescently labeled GW (GW-BODIPY) was encapsulated in the polymeric core of the NP labeled with PLA-Cy5.5 to obtain Col IV-GW-BODIPY-NP. The *Ldlr*^{-/-} mice (*n* = 2 per group) fed a western diet for 14 weeks were injected intravenously with 8 mg of GW per kg body weight in a single dose of fluorescently labeled NPs 4 h prior to tissue collection. B) Relative accumulation of GW-BODIPY and PLA-Cy5.5 in the aorta in comparison to the liver. C) Relative amounts of GW-BODIPY and PLA-Cy5.5 in plasma. D) *Ldlr*^{-/-} mice were fed on a western diet for 14 weeks then switched to a chow diet for another 5 weeks. While on the chow diet, the mice were intravenously injected twice a week with 8 mg kg⁻¹ of body weight (based on the amount of free GW) of free GW, GW-NPs, or Col IV-GW-NPs or PBS (control) to study the effect of the different treatments on plaque macrophage accumulation. E) Representative pictures of aortic roots showing CD68+ cells stained by immunohistochemistry. F) Quantification of the percentage of CD68+ cells in lesion area. G–J) CD68+ cells were isolated by laser capture microscopy to analyze changes on gene expression by qRT-PCR. (PBS, *n* = 8; free GW, *n* = 6; GW-NPs, *n* = 6; Col IV-GW-NPs, *n* = 8) (**p* < 0.05, Col IV-GW-NP group vs. free GW group). Data are expressed as mean ± SEM.

suggesting that GW released from the NPs mediated increased LXR activation in the lesional plaque macrophages ($P = 0.064$ vs. free GW) (Figure 4G). On the other hand, SREBP1c expression was not meaningfully increased in any treatment group, which indicates that SREBP1c processing can be pharmacologically separated from ABCA1 regulation and is independently regulated in plaque macrophages (Figure 4H). Meanwhile, proinflammatory target genes such as MCP-1 or TNF α were downregulated in macrophages treated with free GW, GW-NPs, and Col IV-GW-NPs in advanced atherosclerosis compared to PBS-treated macrophages, demonstrating that GW treatments in general reduced inflammation in atherosclerotic lesions (Figure 4I,J). Taken together, these results indicate that the Col IV targeting ligands of the Col IV-GW-NPs improved the delivery of GW to plaque macrophages, which in turn resulted in activation of LXR signaling and benefits on the content and inflammatory state of plaque macrophages in the *Ldlr*^{-/-} mouse model of atherosclerosis.

2.6. Free GW, but no Col IV-GW-NPs, Alters Hepatic Lipid Metabolism in Mice

A major caveat to the pharmacological use of LXR agonists in the treatment of atherosclerosis is that, despite increasing

cholesterol efflux in plaque macrophages and foam cells, these compounds alter hepatic lipid metabolism by promoting liver steatosis and hypertriglyceridemia.^[39]

To determine whether the NPs mitigate the deleterious effects of GW in mice utilized for therapeutic efficacy studies (Figure 4D), we measured circulating or hepatic TG and cholesterol levels. While circulating TG and cholesterol levels were significantly elevated in mice treated with free GW, mice treated with GW-NPs or Col IV-GW-NPs demonstrated levels comparable to those in the PBS-treated group (Figure 5A,B). Similarly, the TG and cholesterol contents in the liver were not altered in mice treated with GW-NPs or Col IV-GW-NPs (Figure 5C,D). In contrast, free GW treatments elicited a remarkable increase in TG and cholesterol in the liver. These results suggest that the GW encapsulated in the NPs (GW-NPs and Col IV-GW-NPs) does not alter circulating lipid levels or hepatic lipid metabolism while exerting more control over the drug load and release compared to free GW,^[40] avoiding the development of hepatic steatosis in mice undergoing LXR agonist treatment.

We next analyzed changes in LXR-responsive gene expression in liver homogenates to determine the effects of different GW treatments on lipid metabolism. While free GW-treated mice demonstrated significant upregulation of hepatic ABCA1

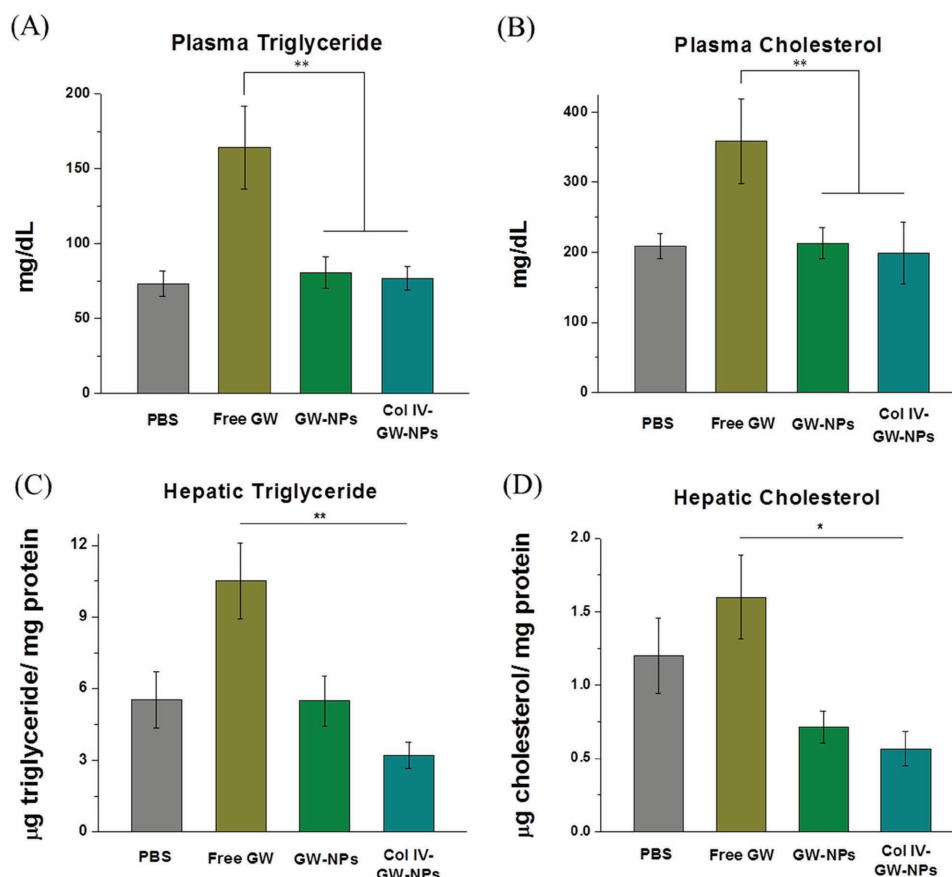


Figure 5. Effects of GW-NPs or Col IV-GW-NPs on circulating and hepatic triglyceride (TG) and cholesterol levels in mice. *Ldlr*^{-/-} mice were fed a western diet for 14 weeks and then switched to a chow diet for another 5 weeks. While on the chow diet, the mice were intravenously injected twice a week with 8 mg kg⁻¹ of body weight (based on the amount of free GW compound) of free GW, GW-NPs, or Col IV-GW-NPs or PBS (control) to study the effect of the different treatments on circulating and hepatic lipid metabolism. A) Plasma TG, B) and plasma cholesterol levels. C) Hepatic TG, D) and hepatic cholesterol levels were calculated from total lipid homogenate. Values refer to the protein content in the homogenate. (PBS, $n = 8$; free GW, $n = 6$; GW-NPs, $n = 9$; Col IV-GW-NPs, $n = 7$) (* $p < 0.05$ and ** $p < 0.01$). Data are expressed as mean \pm SEM.

and ABCG1 compared to mice treated with GW-NPs or Col IV-GW-NPs (Figure 6A,B), no changes in hepatic ABCG5 were noted in any of the treatment groups (Figure 6C). We also measured changes in lipogenic transcription factors such as SREBP1c and fatty acid synthase (FASN), whose expression is regulated by both LXRs and SREBP1.^[41] Similarly, mice treated with free GW showed a substantial increase in hepatic SREBP1c and FASN compared to mice treated with GW-NPs or Col IV-GW-NPs (Figure 6D,E). Last, we measured hepatic mRNA levels of the LXR target cholesterol 7 α -hydroxylase (CYP7a1), which encodes a key enzyme in the pathway converting cholesterol to bile acid.^[42] CYP7a1 levels were higher in mice treated with free GW compared to those treated with Col IV-GW-NPs (Figure 6F).

Collectively, the studies outlined above indicate that free GW promoted hyperlipidemia and elevated cholesterol and TG accumulation in the liver by altering liver lipid metabolism, which poses a significant obstacle to the development of LXR agonists as human therapeutics. However, NPs had no such negative effect, with targeted Col IV-GW-NPs tending to be even more protective against steatosis. For two of the LXR target genes examined, FASN and Cyp7a1, the stimulatory effects of the Col IV-GW-NPs tended to be markedly lower than free GW and also lower than GW-NPs, suggesting that the preferential

accumulation of GW in atherosclerotic aortic lesions in mice treated with Col IV-GW-NPs remarkably reduced the adverse side effects of LXR activation.

3. Conclusion

The unique roles of LXRs as master regulators of the reverse cholesterol transport pathway in lipid homeostasis and inflammation have attracted much attention in the field of drug discovery for the treatment of atherosclerosis. Unfortunately, no LXR agonists have received FDA approval due to the liver toxicity caused by increased hepatic lipogenesis, steatosis, and hyperlipidemia during the treatment. These adverse effects merit innovative strategies to safely activate the LXR pathway. Fortunately, the targeted delivery of LXR agonists using NPs can facilitate effective LXR-mediated therapy while also protecting off-target organs until delivery at the target site. Here we developed GW-encapsulated targeted NPs consisting of PLA core and a lipid layer of DSPE-mPEG1000/DLPC/Col IV-DSPE-PEG2000 with PEG-coating molecules of optimal length on the surface of the NPs to achieve the best combination with the Col IV-targeting ligand linker (Col IV-DSPE-PEG2000). The Col IV-GW-NPs developed here improved GW antiatherogenic

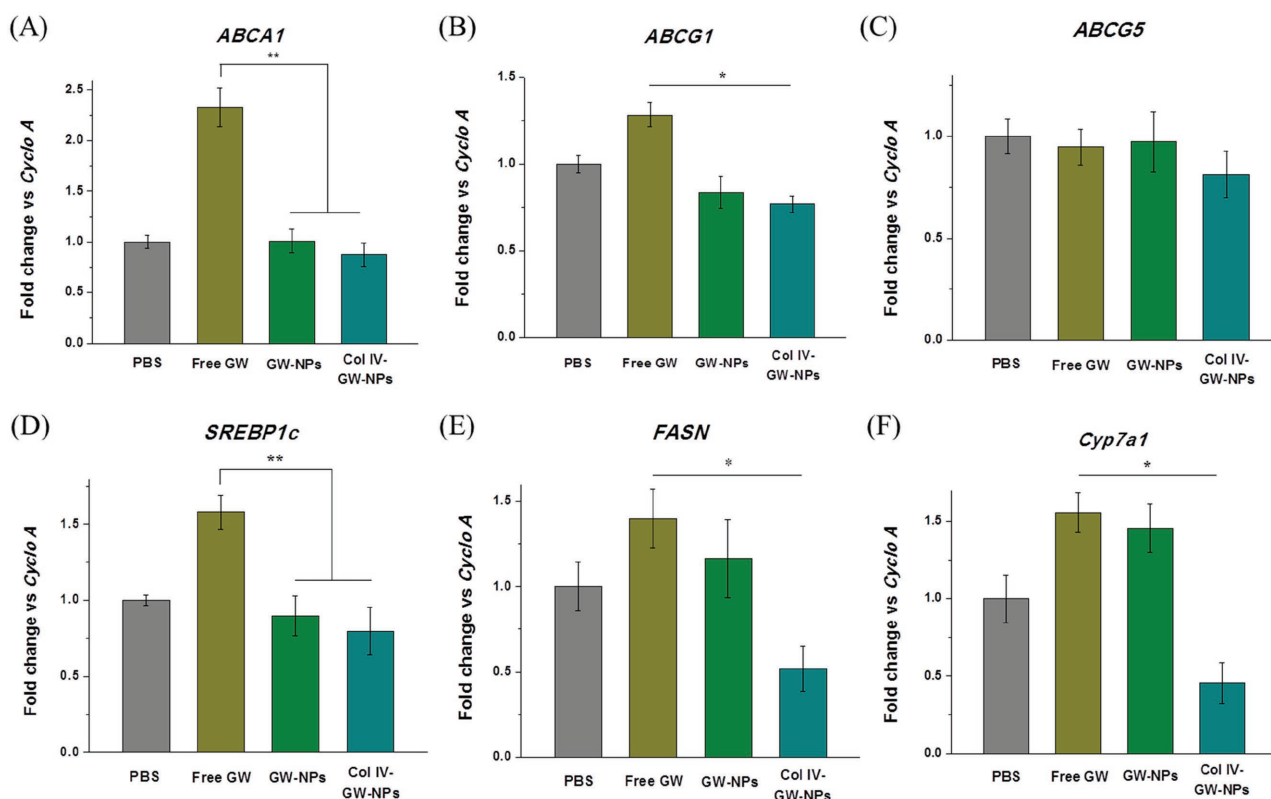


Figure 6. Effects of GW-NPs or Col IV-GW-NPs on hepatic mRNA expression in mice. *Ldlr*^{-/-} mice ($n = 6$ to 9 per group) were fed a western diet for 14 weeks and then switched to a chow diet for another 5 weeks. While on the chow diet, the mice were intravenously injected twice a week with 8 mg kg^{-1} of body weight (based on the amount of free GW) of free GW, GW-NPs, or Col IV-GW-NPs or PBS (control) to study the effects of the different treatments on hepatic lipid expression. Total mRNA was isolated and retrotranscribed to determine the expression levels of selected genes. A) Expression of the ATP-binding cassette A1 (ABCA1), B) ATP-binding cassette G1 (ABCG1), C) ATP-binding cassette G5 (ABCG5), D) sterol regulatory element binding protein (SREBP-1c), E) fatty acid synthase (FASN), and F) cytochrome P450 7A1 (Cyp7a1). Cyclo A was used as a housekeeping control. (PBS, $n = 8$; free GW, $n = 6$; GW-NPs, $n = 9$; Col IV-GW-NPs, $n = 7$) (* $p < 0.05$ and ** $p < 0.01$). Data are expressed as mean \pm SEM.

efficacy without increasing either plasma or liver lipid levels in the *Ldlr*^{-/-} mouse model of atherosclerosis. Our findings indicate that the formulation strategy for atherosclerotic lesion-targeted NPs encapsulating GW may have potential clinical benefits as a LXR-based treatment for atherosclerosis.

4. Experimental Section

Materials: Poly(D,L-lactide) with terminal ester groups (PLA-OCH₃, inherent viscosity 0.26–0.54 dL g⁻¹ in chloroform) was purchased from Durect Lactel Absorbable Polymers (Pelham, AL, USA). PLA with terminal amine groups (PLA-NH₂, M_n 10–15 kDa) was purchased from PolysciTech (IN, USA). DSPE-mPEGs (1,2-distearoyl-sn-glycero-3-phosphoethanolamine-N-[methoxy(polyethylene glycol)]) with PEG molecular weight 550 kDa (DSPE-mPEG550), 1000 kDa (DSPE-mPEG1000), and 2000 kDa (DSPE-mPEG2000), 1,2-distearoyl-sn-glycero-3-phosphoethanolamine-N-[maleimide(polyethylene glycol)-2000] (DSPE-mPEG2000-MAL), 1,2-dilauroyl-sn-glycero-3-phosphocholine (DLPC) were obtained from Avanti Polar Lipids. Cy5.5-NHS monoester was purchased from GE Healthcare Life Sciences. Dimethyl sulfoxide (DMSO), dimethylformamide (DMF), benzyl alcohol, ethyl acetate, acetonitrile (ACN), trifluoroacetic acid (TFA), 1-[Bis(dimethylamino)methylene]-1H-1,2,3-triazolo[4,5-b]pyridinium 3-oxid hexafluorophosphate (HATU), N,N-diisopropylethylamine (DIPEA), and GW3965 (GW) were purchased from Sigma-Aldrich. BODIPY FL EDA, 4,4-difluoro-5,7-dimethyl-4-bora-3a,4a-diaza-s-indacene-3-propionyl ethylenediamine, hydrochloride (BODIPY-NH₂) was purchased from ThermoFisher Scientific (Carlsbad, NY). The Collagen type IV (Col IV)-targeting peptide (KLWVLPKGGGC) was purchased from AnyGen Co., Ltd. (South Korea). ¹H NMR spectra were recorded on a Bruker AVANCE-400 NMR spectrometer. The nanoparticle (NP) sizes and ζ-potentials were obtained by quasi-electric laser light scattering using a ZetaPALS dynamic light-scattering (DLS) detector (15 mW laser, incident beam ¼ 676 nm; Brookhaven Instruments). The NP diameters measured by DLS were displayed as the effective diameters, which were average of the intensity-, volume-, and number-weighted size distributions, calculated based on the Lognormal distribution. Nanoparticle tracking analysis (NTA) for the NPs was performed using Nanosight (Malvern Instruments). Transmission electron microscopy (TEM) was performed on a JEOL 2011 at 200 kV. MALDI TOF mass spectrometry was performed on a Bruker Daltonics. Biacore3000 instrument (Biacore) was used for surface plasmon resonance (SPR) measurement.

Preparation and Characterization of Polymer-Lipid Hybrid NPs: PLA-lipid hybrid NPs with different PEG molecular weights were synthesized from PLA-OCH₃, DSPE-mPEGs (DSPE-mPEG550, DSPE-mPEG1000, DSPE-mPEG2000), and DLPC using a modified single-emulsion technique. PLA-OCH₃, DSPE-mPEGs, and DLPC were dissolved in an organic phase (a mixture of ethyl acetate and benzyl alcohol) and combined with a water phase undergoing high-energy emulsification with a ultrasonic probe sonicator (SONICATOR 4000, MISONIX). NP550, NP1000, and NP2000 were optimized by varying molar ratio of DSPE-mPEGs to DLPC (1:3, 3:7, 7:3, and 10:0) and weight ratio of DSPE-mPEGs/DLPC to PLA (0.5, 0.7, and 1). The PLA/DSPE-mPEGs/DLPC solution with diverse molar ratios of DSPE-mPEG to DLPC and weight ratios of DSPE-mPEGs/DLPC to PLA was added into the water solution dropwise under gentle stirring followed by probe sonication. Then, the NPs were allowed to self-assemble overnight with continuous stirring while the organic phase was allowed to evaporate. The remaining organic solvent and free molecules were removed by washing the NP solution three times using an Amicon Ultra-15 centrifugal filter (EMD Millipore, Germany) with a molecular weight cut-off of 100 kDa and then resuspended in either water or phosphate saline buffer (PBS) to obtain a final desired concentration. The NPs were used immediately or stored at 4 °C. The stability of the NPs in PBS and in 10% fetal bovine serum (FBS)-containing PBS at 37 °C was tested under shaking (100 rpm) with

various incubation times (0–7 d) and the changes in the hydrodynamic size of the NPs were measured by DLS. Samples for TEM were stained with 0.75% uranyl formate or 1% uranyl acetate and measured on a coated copper grid.

Synthesis and Purification of Col IV-DSPE-PEG2000 Conjugate: DSPE-PEG2000-MAL (50 mg, 0.017 mmol) dissolved in chloroform was added the Col IV-targeting peptide (KLWVLPKGGGC, 50 mg, 0.043 mmol) that was previously dissolved in dry DMF. The reaction was stirred at room temperature for 24 h, and then the final product of Col IV-DSPE-PEG2000 conjugate was purified by high-performance liquid chromatography (HPLC; Agilent 1100 (Agilent Technologies, CA)) with a C4 column: 2.2 × 25 cm, gradient: 20–20%/5'–100%/50', A: 0.05% TFA and B: 0.043% TFA, 80% ACN) and characterized by MALDI TOF Mass Spectrometry (average MW found, 4076.9 Da).

Preparation and Characterization of Col IV-NPs: Col IV-NPs were synthesized with a modified single-emulsion method. PLA-OCH₃ was first dissolved in a mixture of ethyl acetate and benzyl alcohol (40 mg mL⁻¹). DSPE-mPEGs, DLPC, and Col IV-DSPE-PEG2000 (67.5:27.5:5, molar ratio) were dissolved in a mixture of ethyl acetate and benzyl alcohol (40 mg mL⁻¹) at 70% of the PLA weight. DSPE-mPEG550, DSPE-mPEG1000, and DSPE-mPEG2000 were used for the preparation of Col IV-NP(550), Col IV-NP(1000), and Col IV-NP(2000), respectively. The PLA/lipid mixture in a cosolvent of ethyl acetate and benzyl alcohol was then added into the aqueous solution (Hyclone, molecular biology-grade water) dropwise under gentle stirring followed by probe sonication. Then the NPs were purified by washing with Amicon Ultra-15 centrifugal filter (molecular weight cutoff of 100 kDa). Stability of the NPs in PBS and in 10% FBS at 37 °C was tested under shaking (100 rpm) with various incubation times (0–7 d), and changes in the hydrodynamic size of the NPs were measured by DLS.

Preparation and Characterization of GW-NPs and Col IV-GW-NPs: PLA-OCH₃ was dissolved in a cosolvent of ethyl acetate and benzyl alcohol (40 mg mL⁻¹). For the preparation of GW-NP and Col IV-GW-NP, DSPE-mPEG1000/DLPC (7:3, molar ratio) and DSPE-mPEG1000/DLPC/Col IV-DSPE-PEG2000 (67.5:27.5:5, molar ratio), respectively, were dissolved in a cosolvent of ethyl acetate and benzyl alcohol (40 mg mL⁻¹) at 70% of the PLA weight. GW dissolved in DMSO was added to the PLA/lipid mixture solution at 20% of the total weight. The PLA/lipid/drug mixture in organic phase was then added into the aqueous solution dropwise under gentle stirring followed by probe sonication. Then the NPs were purified by washing the NP solution four times using an Amicon Ultra-15 centrifugal filter (molecular weight cutoff of 100 kDa). Hydrodynamic size and surface charge were analyzed by DLS. Drug-loading amount of the NPs was analyzed using HPLC.

Nanoparticle SPR Measurements: The binding of NPs to Col IV was measured on a Biacore3000 instrument using CM5 sensor chips. The surface carboxyl groups of CM5 chip were activated with 1:1 0.4 M 1-ethyl-3-(3-dimethylaminopropyl) carbodiimide (EDC)/0.1 M NHS. 25 µg mL⁻¹ solution of human collagen IV in acetate buffer pH 5.0 was manually flowed to make 600 RU, 1600 RU, 3000 RU for several minutes at a rate of 5 µL min⁻¹ over 2, 3, and 4 channel (1 is reference without Col IV). The remaining NHS-ester groups on the sensor surface were quenched with a 7 min injection of 1.0 M ethanolamine. Binding of NPs was assessed as a function of concentration in PBS-P+ buffer (sample injection: 40 µg min⁻¹, 60 µL). Serial dilutions of the NPs were performed to prepare samples with different concentrations (0.3–5 mg mL⁻¹) before measurement. EDTA regeneration was used to wash bound NPs before starting the next set of experiments.

Drug Release Kinetics Study: NPs were suspended in water and aliquoted into several semipermeable minidialysis tubes (Slide-A-Lyzer, MWCO: 10 kDa, ThermoFisher Scientific). The dialysis tubes were placed in 2 L of PBS (pH 7.4) at 37 °C. At defined time intervals, NPs in each tube were collected and prepared in ACN:water (1:1, v/v) and 0.01 × 10⁻³ M NaOH for HPLC measurement. The remaining drug in NPs at different time points was quantified by HPLC (C18 column: 4.6 × 15 cm, gradient: 20–80%/5'–80%/30', A: water and B: ACN).

Synthesis of GW-BODIPY: The liver X receptor (LXR) synthetic agonist GW (25 mg, 40 µmol) was dissolved in dry DMF (500 µL); to this was

added HATU (30 mg, 80 μ mol) in dry DMF (100 μ L), and the reaction was stirred for 20 min. Subsequently, BODIPY-NH₂ (5 mg, 13.5 μ mol) in dry DMF (500 μ L) and DIPEA (54 μ mol) were added. The reaction was stirred overnight at room temperature. The GW-BODIPY conjugate was purified using HPLC (C18 column, gradient: 0–0.01% 100%/60', A: 0.05% TFA and B: 0.043% TFA, 80% ACN) and characterized by ¹H NMR and MALDI TOF Mass Spectrometry. ¹H NMR (400 MHz, CDCl₃): δ 8.72, 8.68 (1H, 2 x –NH–C=O), 8.49–7.74 (BODIPY and GW rings), 7.80–6.36 (BODIPY and GW rings), 5.28 (s, 1H, –C=C–H), 3.4–3.18 (m, 8H, –CH₂–), 2.65–2.57 (–CH₂–CH₂–N– and –N–CH₂–CH–), 2.45 (–CH₂–CH₂–C=O), 2.34 (sharp s, 6H, –CH₃ x 2), 1.84 (m, 6H, –O–C H₂–CH₂–CH₂–) ppm. HRMS (MALDI) calculated for C₄₈H₄₈BClF₅N₅O₃ [M]⁺, 883.35; found, 884.766.

Synthesis of PLA-Cy5.5: PLA-NH₂ (6.8 mg, 0.65 μ mol) dissolved in dry DMF (10 mg mL^{–1}) was added to Cy5.5-NHS mono ester (1 mg, 1.3 μ mol) that was dissolved in dry DMF (10 mg mL^{–1}). The reaction was stirred overnight at RT and purified by dialysis membrane (MWCO 3.5 kDa).

Cell Culture Experiments: Peritoneal macrophages were obtained from C57BL/6 mice by inducing sterile peritonitis with intraperitoneal injection of 3 mL of 4% Brewers thioglycollate medium 72 h before harvest. Mice were humanely euthanized and macrophages were extracted from the peritoneal cavity by lavage with 10 mL sterile PBS (pH 7.4) three times. The resulting exudate was pelleted, and cells were washed twice with PBS. Cells were maintained in Dulbecco's minimal essential medium (DMEM) supplemented with 10% FBS (Gemini, CA), penicillin/streptomycin (100 U mL^{–1}; 100 μ g mL^{–1}, Sigma), and 4 \times 10^{–3} M L-glutamine (ATCC, Manassas, VA) at 37 °C in a humidified 5% CO₂ atmosphere. After plating in 12-well plates, cells were incubated for 1 h to allow macrophages to adhere, washed three times with PBS, and cultured in complete medium. Peritoneal macrophages were used to determine the efficacy of the different NP formulations on gene expression. Cells were exposed for 18 h to GW-NP, Col IV-GW-NP, or free GW dissolved in DMSO at an equivalent concentration of 1 \times 10^{–6} M of GW. PBS was used as a negative control.

Flow Cytometry: Peritoneal macrophages were grown as described above and treated with rhodamine-labeled NPs or Col IV-NPs (20 μ g rhodamine mL^{–1}) for 4 h. Macrophages were identified by staining with BV650 antimouse CD11b (Biolegend, San Diego, CA) and PE/Cy7 antimouse F4/80 (Biolegend). Rhodamine (Excitation/Emission; 560 nm/583 nm) intensities within macrophages were quantified using the LSRII analyzer system (BD biosciences, Franklin Lakes, NJ).

Nanoparticle Uptake: To determine the internalization pathway of the NPs by macrophages, we incubated peritoneal macrophages with the corresponding inhibitors (filipin: 1 μ g mL^{–1}; chlorpromazine (CPZ): 10 μ g mL^{–1}; cytochalasin D (CytD): 0.5 μ g mL^{–1}; Latrunculin A (LatA): 0.025 μ g mL^{–1}) for 1 h prior adding the rhodamine-labeled NPs for one extra hour. After the incubation, cells were washed twice with fluorescence-activated cell sorting (FACS) buffer (PBS + 1% BSA) and stained with the corresponding antibodies to determine the uptake efficiency.

Confocal Microscopy: Peritoneal macrophages were grown on glass coverslips as described above. Cells were treated with rhodamine-labeled NPs or Col IV-NPs (20 μ g rhodamine mL^{–1}) for 4 h. After incubation, cells were fixed with 10% buffered formalin (Sigma) and washed with PBS. DAPI was used to stain nuclei. Confocal images were acquired with a Leica TCS SP5 II confocal microscope using a 405 diode laser (excitation 405 nm) and two He-Ne lasers (excitation 543 and 633 nm) with a 63 \times Apochromat, numerical aperture 1.40-Oil objective.

Animals and Diets: All mice used in this study were on the C57BL/6 background and obtained from Jackson Laboratories (Bar Harbor, Maine). Mice were allowed free access to food and water, and all in vivo studies were performed in accordance with the New York University Institutional Animal Care and Use Committee as well as the National Institutes of Health Animal guidelines. Atherosclerosis studies were performed using low-density lipoprotein receptor knockout mice (*Ldlr*^{–/–}), which develop complex atherosclerotic lesions in the vasculature when fed a high-cholesterol diet. Mice were weaned 4 weeks

after birth onto a western diet (21% fat supplemented with 0.15% cholesterol wt/wt; Dyets, Bethlehem, PA). After 14 weeks on the western diet, mice were switched to a standard chow diet (5% fat and 0.01% of cholesterol wt/wt; LabDiet, St. Louis, MO) and free GW, GW-NPs, and Col IV-GW-NPs were injected intravenously through the retro-orbital sinus with 8 mg kg^{–1} of body weight (based on the concentration of GW compound). Treatments were administered twice a week over a span of 5 weeks. The last injection was administered 4 h prior to sacrifice. Mice were euthanized at the completion of treatment with a peritoneal injection of ketamine/xylazine, and blood was collected in EDTA-containing tubes via cardiac puncture for plasma analyses. Mice were then perfused with 10% sucrose in saline solution (0.9% NaCl in water), after which organs were harvested. Aortic roots were embedded in optimal cutting temperature (OCT) compound (Sakura, Torrance, CA), and OCT blocks immediately frozen at –80 °C. Portions of liver were snap-frozen in liquid nitrogen and subsequently stored at –80 °C.

In Vivo Biodistribution: *Ldlr*^{–/–} mice were weaned 4 weeks after birth onto a western diet to induce atherosclerotic lesions in the aorta. After 14 weeks, mice were injected with the GW-BODIPY-NPs or Col IV-GW-BODIPY-NPs (8 mg of GW-BODIPY/kg) and sacrificed at 4 h postinjection. After perfusion, the whole aorta (from the aortic root to the iliac bifurcation), liver, and plasma were collected and visualized using the IVIS 200 in vivo imaging system (Perkin Elmer, MA). The fluorescence intensities from the NPs (Cy5.5; excitation/emission 675 nm/720 nm) and the GW (BODIPY; excitation/emission 460 nm/520 nm) were quantified as total radiant efficiency (TRE), following manufacturer's instructions. The values are represented as the ratio of the TRE in the aorta normalized by the TRE present in the liver for each fluorophore.

Immunohistochemistry: OCT blocks containing the aortic roots were sectioned at 6 μ m thickness and mounted on glass slides. To detect CD68+ cells in the atherosclerotic lesions, sections were fixed in 100% acetone and stained for CD68+ using primary rat antimouse CD68 antibody (Bio-Rad, CA), followed by biotinylated antirat IgG secondary antibody (Vector Laboratories, CA), and further visualized using a Vectastain ABC kit (Vector Laboratories). Specimens were subsequently counterstained with hematoxylin/eosin (Sigma), dehydrated using xylene (Fisher Scientific, NH) and mounted with coverslips using Permount (Fisher Scientific). Morphometric analyses were performed using ImageProPlus 7 (Micro Optical Solutions LCC, MA) on bright field images of stained sections at 10 \times magnification. Total lesion area and CD68+ area were used to determine the percentage of CD68+ staining in the atherosclerotic lesions.

Laser Capture Microdissection: RNA from CD68+ cells was isolated from atherosclerotic plaques using LCM, as previously described.^[43] Briefly, aortic root sections were stained with hematoxylin/eosin in RNase-free conditions to further isolate the CD68+ cells using consecutive guiding sections previously stained for CD68+ cells as described above. CD68+ cells from the same sample were pooled to isolate and purify the RNA using the PicoPure Kit (ThermoFisher Scientific). The quality and quantity of the RNA samples were determined using an Agilent 2100 Bioanalyzer (Agilent Technologies). RNA was converted to cDNA and amplified using the WT-Ovation Pico RNA Amplification Kit (NuGEN, San Carlos, CA). Real-time PCR analyses were performed using 5 ng of amplified cDNA in the Quantstudio 7 Flex (Applied Biosystems) (see below).

RNA Isolation in Cell Culture and Liver: Total RNA from tissue samples or cells was obtained using TRIzol reagent (Thermo Scientific) following the manufacturer's instructions. Once isolated and purified, the RNA concentration was determined with NanoDrop (Thermo Scientific) and reverse-transcribed using the Verso cDNA kit (Thermo Scientific, Carlsbad, CA).

Real-Time PCR Analyses: Quantitative real-time PCR was performed with Taqman Gene Expression Master Mix (Applied Biosystems, Foster City, CA), and Taqman primer/probe mixes for ATP binding cassette transporter subfamily A member 1 (ABCA1), ATP binding cassette transporter subfamily G member 1 (ABCG1), sterol-regulatory binding protein 1c (SREBP1c), monocyte chemoattractant protein 1 (MCP-1),

ATP binding cassette transporter subfamily G member 5 (ABCG5), fatty acid synthase (FAS), and cytochrome P450 7A1 (CYP7A1) were used. Gene expression was assessed using the $\Delta\Delta C_t$ calculation method using hypoxanthine-guanine phosphoribosyltransferase (HPRT) as a housekeeping gene for LCM-isolated CD68+ cells, and cyclophilin A (Cyclo A) was used as housekeeping gene for the rest of the experiments.

Lactate Dehydrogenase Toxicity Assay: The toxicity of the different treatments in cell culture experiments was tested by colorimetric quantification of lactate dehydrogenase (LDH) release into medium following manufacturer's instructions (Thermo Scientific, Carlsbad, CA).

Cholesterol and Triglyceride Measurements: Liver samples were weighed and homogenized in PBS. A fraction of the total homogenate was incubated with 3 mL of isopropanol (Sigma) overnight at 4 °C to extract the total lipid content. The solvent/lipid mixture was centrifuged at 3000 × g for 10 min, the supernatant was then collected in glass tubes, dried under a stream of nitrogen, and resuspended in equal volumes of isopropanol. Total triglyceride and cholesterol measurements were performed using standard colorimetric assays (Wako) following manufacturer's directions. Total protein in the homogenate was measured by a Lowry assay (BioRad) to normalize the triglyceride and cholesterol levels.

Statistical Analysis: Data are expressed as mean ± SEM and analyzed by one-way ANOVA as appropriate for multiple comparisons. A *P* value less than 0.05 was considered significant.

Supporting Information

Supporting Information is available from the Wiley Online Library or from the author.

Acknowledgements

M.Y. and J.A. contributed equally to this work. This research was supported by the NHLBI Program of Excellence in Nanotechnology (PEN) contract HHSN268201000045C (E.A.F., O.C.F.) from the National Heart, Lung, and Blood Institute, National Institute of Health (NIH). O.C.F. acknowledges NIH support from grants HL127464; the National Research Foundation of Korea K1A1A2048701; and the David Koch-Prostate Cancer Foundation Award in Nanotherapeutics. These studies were also supported by NIH grants HL117226, and HL084312, and Department of Defense grant PR151468 (E.A.F.). J.A. is a recipient of a Scientist Development Grant from the American Heart Association (16SDG27550012). A.M. was supported by an NYU training grant T32HL098129.

Conflict of Interest

In compliance with the Brigham and Women's Hospital and Harvard Medical School institutional guidelines, O.C.F. discloses his financial interest in Selecta Biosciences, Tarveda Therapeutics, and Placon Therapeutics. These companies did not support the aforementioned research and currently have no rights to any technology or intellectual property developed as part of this research. The rest of the authors declare no conflicts of interest.

Keywords

atherosclerosis, GW3965, liver X receptor (LXR), nanoparticles, targeted drug delivery

Received: March 10, 2017
Revised: April 27, 2017
Published online: July 21, 2017

- [1] P. Libby, I. Tabas, G. Fredman, E. A. Fisher, *Circ. Res.* **2014**, *114*, 1867.
- [2] S. D. Lee, P. Tontonoz, *Atherosclerosis* **2015**, *242*, 29.
- [3] A. R. Tall, L. Yvan-Charvet, *Nat. Rev. Immunol.* **2015**, *15*, 104.
- [4] A. Grefhorst, B. M. Elzinga, P. J. Voshol, T. Plösch, T. Kok, V. W. Bloks, F. H. van der Sluijs, L. M. Havekes, J. A. Romijn, H. J. Verkade, F. Kuipers, *J. Biol. Chem.* **2002**, *277*, 34182.
- [5] S. B. Joseph, E. McKilligin, L. Pei, M. A. Watson, A. R. Collins, B. A. Laffitte, M. Chen, G. Noh, J. Goodman, G. N. Hagger, J. Tran, T. K. Tippin, X. Wang, A. J. Lusis, W. A. Hsueh, R. E. Law, J. L. Collins, T. M. Willson, P. Tontonoz, *Proc. Natl. Acad. Sci. USA* **2002**, *99*, 7604.
- [6] J. R. Schultz, H. Tu, A. Luk, J. J. Repa, J. C. Medina, L. Li, S. Schwendner, S. Wang, M. Thoolen, D. J. Mangelsdorf, K. D. Lustig, B. Shan, *Genes Dev.* **2000**, *14*, 2831.
- [7] M. Orditura, F. Quaglia, F. Morgillo, E. Martinelli, E. Lieto, G. De Rosa, D. Comunale, M. R. Diadema, F. Ciardiello, G. Catalano, F. De Vita, *Oncol. Rep.* **2004**, *12*, 549.
- [8] M. E. O'Brien, N. Wigler, M. Inbar, R. Rosso, E. Grischke, A. Santoro, R. Catane, D. G. Kieback, P. Tomczak, S. P. Ackland, F. Orlandi, L. Mellars, L. Alland, C. Tendler, *Ann. Oncol.* **2004**, *15*, 440.
- [9] J. E. Lancet, G. L. Uy, J. E. Cortes, L. F. Newell, T. L. Lin, E. K. Ritchie, K. R. Stuart, S. A. Strickland, D. Hogge, S. R. Solomon, R. M. Stone, D. L. Bixby, J. E. Kolitz, G. J. Schiller, M. J. Wieduwilt, D. H. Ryan, A. Hoering, M. Chiarella, A. C. Louie, B. C. Medeiros, H. Lee, *J. Clin. Oncol.* **2016**, *34*, suppl. Abstr. 7000.
- [10] US National Library of Medicine. *ClinicalTrials.gov* <https://clinicaltrials.gov/ct2/show/NCT02213744?term> (accessed: January 2017).
- [11] US National Library of Medicine. *ClinicalTrials.gov* <https://clinicaltrials.gov/ct2/show/NCT00964080?term> (accessed: November 2014).
- [12] W. J. Mulder, F. A. Jaffer, Z. A. Fayad, M. Nahrendorf, *Sci. Transl. Med.* **2014**, *6*, 239sr1.
- [13] C. Tarin, M. Carril, J. L. Martin-Ventura, I. Markuerkiaga, D. Padro, P. Llamas-Granda, J. A. Moreno, I. García, N. Genicio, S. Plaza-Garcia, L. M. Blanco-Colio, S. Penades, J. Egido, *Sci. Rep.* **2015**, *5*, 17135.
- [14] S. Gadde, O. Even-Or, N. Kamaly, A. Hasija, P. G. Gagnon, K. H. Adusumilli, A. Erakovic, A. K. Pal, X. Q. Zhang, N. Kolishetti, J. Shi, E. A. Fisher, O. C. Farokhzad, *Adv. Healthcare Mater.* **2014**, *3*, 1448.
- [15] X. Q. Zhang, O. Even-Or, X. Xu, M. van Rosmalen, L. Lim, S. Gadde, O. C. Farokhzad, E. A. Fisher, *Adv. Healthcare Mater.* **2015**, *4*, 228.
- [16] J. M. Chan, L. Zhang, R. Tong, D. Ghosh, W. Gao, G. Liao, K. P. Yuet, D. Gray, J. W. Rhee, J. Cheng, G. Golomb, P. Libby, R. Langer, O. C. Farokhzad, *Proc. Natl. Acad. Sci. USA* **2010**, *107*, 2213.
- [17] N. Kamaly, G. Fredman, M. Subramanian, S. Gadde, A. Pesic, L. Cheung, Z. A. Fayad, R. Langer, I. Tabas, O. C. Farokhzad, *Proc. Natl. Acad. Sci. USA* **2013**, *110*, 6506.
- [18] G. Fredman, N. Kamaly, S. Spolitu, J. Milton, D. Ghorpade, R. Chiasson, G. Kuriakose, M. Perretti, O. Farokhzad, I. Tabas, *Sci. Transl. Med.* **2015**, *7*, 275ra20.
- [19] N. Kamaly, G. Fredman, J. J. Foias, M. Subramanian, W. I. Choi, K. Zepeda, C. Vilos, M. Yu, S. Gadde, J. Wu, J. Milton, R. Carvalho Leitao, L. Rosa Fernandes, M. Hasan, H. Gao, V. Nguyen, J. Harris, I. Tabas, O. C. Farokhzad, *ACS Nano* **2016**, *10*, 5280.
- [20] J. M. Chan, L. Zhang, K. P. Yuet, G. Liao, J. W. Rhee, R. Langer, O. C. Farokhzad, *Biomaterials* **2009**, *30*, 1627.
- [21] J. Wu, N. Kamaly, J. Shi, L. Zhao, Z. Xiao, G. Hollett, R. John, S. Ray, X. Xu, X. Zhang, P. W. Kantoff, O. C. Farokhzad, *Angew. Chem., Int. Ed. Engl.* **2014**, *53*, 8975.
- [22] X. Zhu, Y. Xu, L. M. Solis, W. Tao, L. Wang, C. Behrens, X. Xu, L. Zhao, D. Liu, J. Wu, N. Zhang, I. I. Wistuba, O. C. Farokhzad, B. R. Zetter, J. Shi, *Proc. Natl. Acad. Sci. USA* **2015**, *112*, 7779.

- [23] Q. Dai, C. Walkey, W. C. Chan, *Angew. Chem., Int. Ed. Engl.* **2014**, 53, 5093.
- [24] J. F. Stefanick, J. D. Ashley, T. Kiziltepe, B. Bilgicer, *ACS Nano* **2013**, 7, 2935.
- [25] J. F. Stefanick, J. D. Ashley, B. Bilgicer, *ACS Nano* **2013**, 7, 8115.
- [26] P. E. Saw, J. Park, E. Lee, S. Ahn, J. Lee, H. Kim, J. Kim, M. Choi, O. C. Farokhzad, S. Jon, *Theranostics* **2015**, 5, 746.
- [27] F. Huang, M. You, T. Chen, G. Zhu, H. Liang, W. Tan, *Chem. Commun.* **2014**, 50, 3103.
- [28] L. Zhang, J. M. Chan, F. X. Gu, J. W. Rhee, A. Z. Wang, A. F. Radovic-Moreno, F. Alexis, R. Langer, O. C. Farokhzad, *ACS Nano* **2008**, 2, 1696.
- [29] C. Pfeiffer, C. Rehbock, D. Hühn, C. Carrillo-Carrion, D. J. de Aberasturi, V. Merk, S. Barcikowski, W. J. Parak, *J. R. Soc. Interface* **2014**, 11, 20130931.
- [30] L. Zhang, D. Zhu, X. Dong, H. Sun, C. Song, C. Wang, D. Kong, *Int. J. Nanomed.* **2015**, 10, 2101.
- [31] Y. Guo, L. Wang, P. Lv, P. Zhang, *Oncol. Lett.* **2015**, 9, 1065.
- [32] J. Gao, Y. Xia, H. Chen, Y. Yu, J. Song, W. Li, W. Qian, H. Wang, J. Dai, Y. Guo, *Nanomedicine* **2014**, 9, 279.
- [33] C. Tassa, J. L. Duffner, T. A. Lewis, R. Weissleder, S. L. Schreiber, A. N. Koehler, S. Y. Shaw, *Bioconjugate Chem.* **2010**, 21, 14.
- [34] A. Kelsch, S. Tomcin, K. Rausch, M. Barz, V. Mailänder, M. Schmidt, K. Landfester, R. Zentel, *Biomacromolecules* **2012**, 13, 4179.
- [35] C. Hong, P. Tontonoz, *Nat. Rev. Drug Discovery* **2014**, 13, 433.
- [36] J. J. Repa, G. Liang, J. Ou, Y. Bashmakov, J. M. Lobaccaro, I. Shimomura, B. Shan, M. S. Brown, J. L. Goldstein, D. J. Mangelsdorf, *Genes Dev.* **2000**, 14, 2819.
- [37] A. Ito, C. Hong, X. Rong, X. Zhu, E. J. Tarling, P. N. Hedde, E. Gratton, J. Parks, P. Tontonoz, *eLife* **2015**, 4, e08009.
- [38] F. K. Swirski, P. Libby, E. Aikawa, P. Alcaide, F. W. Lusinskas, R. Weissleder, M. J. Pittet, *J. Clin. Invest.* **2007**, 117, 195.
- [39] J. R. Schultz, H. Tu, A. Luk, J. J. Repa, J. C. Medina, L. Li, S. Schwendner, S. Wang, M. Thoolen, D. J. Mangelsdorf, K. D. Lustig, B. Shan, *Genes Dev.* **2000**, 14, 2831.
- [40] F. B. Bombelli, C. A. Webster, M. Moncrieff, V. Sherwood, *Lancet Oncol.* **2014**, 15, e22.
- [41] S. B. Joseph, B. A. Laffitte, P. H. Patel, M. A. Watson, K. E. Matsukuma, R. Walczak, J. L. Collins, T. F. Osborne, P. Tontonoz, *J. Biol. Chem.* **2002**, 277, 11019.
- [42] D. J. Peet, S. D. Turley, W. Ma, B. A. Janowski, J. M. Lobaccaro, R. E. Hammer, D. J. Mangelsdorf, *Cell* **1998**, 93, 693.
- [43] J. E. Feig, E. A. Fisher, *Methods Mol. Biol.* **2013**, 1027, 123.